



Acoustic detection of zooplankton diel vertical migration behaviors on the northern Gulf of Mexico shelf

Sabrina M. Parra^{1,a*}, Adam T. Greer², Jeffrey W. Book³, Alison L. Deary^{4,b}, Inia M. Soto^{2,c},
Carla Culpepper⁴, Frank J. Hernandez⁴, Travis N. Miles⁵

¹American Society for Engineering Education, Stennis Space Center, Mississippi

²Division of Marine Science, The University of Southern Mississippi, Stennis Space Center, Mississippi

³U.S. Naval Research Laboratory, Stennis Space Center, Mississippi

⁴Division of Coastal Sciences, The University of Southern Mississippi, Ocean Springs, Mississippi

⁵School of Environmental and Biological Sciences, Rutgers University, New Brunswick, New Jersey

Abstract

Zooplankton respond to light levels, oceanographic conditions, and other cues through diel vertical migrations (DVMs), which can occur at dawn and dusk. However, unraveling the influence of these drivers is difficult without high-resolution time series data encompassing multiple events that can alter zooplankton DVM. We address this knowledge gap with an interseasonal study using high-resolution measurements of zooplankton DVMs on the freshwater-influenced northern Gulf of Mexico shelf. Sampling encompassed 6 months of acoustic backscatter and vertical velocity profiles at five locations, supplemented with zooplankton taxonomic composition and abundance from in situ imaging, net samples, glider profiles, and remote sensing. Relative backscatter anomalies (RBAs) displayed a daily pattern that changed abruptly at dawn and dusk, with lower daytime (2–15 dB lower) values relative to nighttime. Daily variability intensified from autumn to spring. The DVM pattern changed in structure on shorter temporal scales (days to weeks), associated with factors including onshore and off-shelf currents, lunar variability, cloud cover, and harmful algal bloom passage. In situ imaging and net observations showed that the most likely acoustically observed migrating zooplankton were chaetognaths, shrimp (performing reverse DVMs), copepods, and ostracods. Shrimp and chaetognath orientations also showed diel variability, with individuals more frequently oriented vertically during the daytime. Daily RBA and vertical velocity anomaly patterns could be caused by reverse DVM to the near-surface or nocturnal DVM to the near-bottom (outside the acoustic detection range) or diel changes in organism orientation. Pattern complexities suggest that multiple behaviors are happening and being observed simultaneously.

Diel vertical migration (DVM) is a ubiquitous behavior in organisms observed throughout the world's aquatic systems. Two predominant behavioral patterns have been described: nocturnal and reverse DVM (Neilson and Perry 1990). Nocturnal

DVM is the most commonly observed pattern that involves the upward movement of organisms at dusk and downward at dawn (Hutchinson 1967; Lampert 1989; Brierley 2014). Reverse DVM is the upward migration of organisms at dawn and downward at dusk (Heywood 1996; Pearre 2003; Cohen and Forward 2009). Another form of DVM includes the dispersing of organisms throughout the water column at night and retreating to the very bottom (nocturnal) or surface (reverse) during the day (Brewer and Kleppel 1986; Heath et al. 1988; Lyczkowski-Shultz and Steen 1991). DVM behavior is generally thought to maximize ecological benefits (such as access to prey) while minimizing costs (such as mortality risk) (Hays 2003)—a framework known as Gilliam's rule (Gilliam and Fraser 1987; Leonardsson 1991; Loose and Dawidowicz 1994). The benefits to performing DVMs include reduced light-dependent mortality risk and potential access to higher abundances of prey, whereas the costs are energy expenditures through swimming and reduced growth rates caused by temperature changes (Lampert 1989). Although

*Correspondence: sabrina.parra@usm.edu

This is an open access article under the terms of the Creative Commons Attribution License, which permits use, distribution and reproduction in any medium, provided the original work is properly cited.

Additional Supporting Information may be found in the online version of this article.

Present address:

^aDivision of Marine Science, The University of Southern Mississippi, Stennis Space Center, Mississippi

^bAlaska Fisheries Science Center, National Oceanic and Atmospheric Administration, Seattle, Washington

^cHarte Research Institute for Gulf of Mexico Studies, Texas A&M University, Corpus Christi, Texas

there are numerous environmental factors influencing DVMs, evidence suggests that the most common driver is predator evasion (Stich and Lampert 1981; Hays 2003; Pearre 2003).

The primary physical factor that influences DVM is ambient light intensity (Cohen and Forward 2009; Aksnes et al. 2017), with other modulating factors such as currents, turbulence, and stratification (Wiebe et al. 1979; Pagès and Gili 1991; Hamner 1995). Longer periods of DVM variability have been observed through light intensity changes in seasonal (Ochoa et al. 2013; van Haren and Compton 2013; Valle-Levinson et al. 2014) and lunar time scales (van Haren 2007; Hernández-León et al. 2010; Ochoa et al. 2013). However, these longer periods of variability typically cannot be resolved with time-limited, ship-based oceanographic sampling.

DVMs can be studied with acoustic measurements in tandem with depth-discrete net samplers. A commonly used acoustic instrument for estimating zooplankton abundances is the echosounder. Generally, it employs multiple acoustic frequencies to estimate abundances and sizes of organisms through calibration between the acoustic mean volume backscattering strength and organism abundances derived from net samples. An acoustic signal can also be obtained from an acoustic Doppler current profiler (ADCP), an instrument primarily used to study ocean currents (Teledyne 2011). The ADCP's acoustic signal can also be calibrated to provide a mean volume backscattering strength (using a single frequency) (Griffiths and Diaz 1996), as ADCPs have been used to describe distributions and behaviors of zooplankton in different oceanographic environments (e.g., Heywood 1996; Tarling et al. 2002; Ochoa et al. 2013).

The longer term measurements that can be made from moored acoustic instruments allow for a thorough investigation of the spatiotemporal behavioral patterns using data analysis techniques generally reserved for physical processes. However, ADCPs have poor taxonomic resolution, only capable of detecting within a certain target size range depending on the instrument frequency (Benoit-Bird and Lawson 2016). Additionally, ADCPs are not usually calibrated to provide quantitative estimates of zooplankton concentrations, unlike echosounders. Therefore, concurrent biological sampling, preferably on similar spatial scales, is necessary to identify the likely scatterers of longer term acoustic measurements (Jiang et al. 2007; Barth et al. 2014).

Net samples or ADCPs have been used to observe zooplankton DVMs in the Gulf of Mexico. For example, larval red drum perform both nocturnal (Holt and Holt 2000) and reverse (Lyczkowski-Shultz and Steen 1991) DVMs. In both instances, low vertical and temporal resolution nets were used and no measured oceanographic properties explained the DVM patterns. Larvae of Atlantic Croaker undergo reverse DVM in the Mississippi Bight region of the Gulf of Mexico (shelf east of the Mississippi River Delta), also with no clear environmental driver for their behavior as studied with low-resolution net samples (Comyns and Lyczkowski-Shultz 2004). Conversely, Ochoa et al. (2013) used high spatiotemporal resolution ADCPs to qualitatively describe the diel migration patterns in

the eastern Gulf of Mexico and found that zooplankton DVMs vary seasonally and with the lunar cycle from 250 to > 1000 m excursion depths. However, there was no validation using other methods of biological sampling. Discrepancies among these studies suggest that multiple environmental drivers may operate at varying spatiotemporal scales to influence distributions of planktonic organisms and require interdisciplinary sampling approaches to resolve the different scales of variability (Pearre 2003). Vertical migration behaviors have important implications for the transport of planktonic organisms (Farmer and Freeland 1983; Paris and Cowen 2004), but few studies include both high-resolution spatiotemporal data with high taxonomic resolution.

River plumes encountering shelf seas create complex near-shore hydrodynamics that provide an influx of nutrients, leading to increases in abundances for zooplankton (Winder et al. 2017) and higher trophic levels. The Mississippi Bight, located on the northern Gulf of Mexico shelf, is dominated by numerous riverine outflow plumes, with the most significant being those from the Mississippi River and Mobile Bay. Plumes react quickly to wind forcing, which mixes with shelf waters (Dzwonkowski et al. 2011, 2017; Schiller et al. 2011). Proximity to these plumes alters the migration patterns as observed in acoustic backscatter measurements (Pearre 2003; Sindlinger et al. 2005). Here, we bridge the shortcomings of biologically descriptive, low spatiotemporal resolution taxonomic samples with nondescript, high spatiotemporal resolution ADCP profiles of relative backscatter, and vertical velocity.

In some instances, the presence of harmful algal blooms (HABs) could also affect zooplankton behavior. For example, blooms of the toxic dinoflagellate *Karenia brevis* influence the swimming behavior of copepods (Cohen et al. 2007; Hong et al. 2012). *K. brevis*, found on the northeastern Gulf of Mexico shelf, exhibits reverse DVMs concentrated within the top 10 m (Heil et al. 2014; Hu et al. 2016). Although certain nonselective zooplankton grazers will feed on *K. brevis* (Turner and Tester 1989; Hansen et al. 1998), others have reduced abundances during *K. brevis* blooms (Lester et al. 2008), likely due to lethal or sublethal physiological effects of brevetoxin on grazers (Kubanek et al. 2007).

A combination of moored and towed instrumentation can allow for high spatiotemporal resolution and an ability to identify the composition of the scatterers. We incorporated data from multiple samplers to describe interseasonal and higher spatiotemporal resolution environmental impacts on DVM patterns. The observations focused on qualitative analysis of the diurnal signal in the relative backscatter anomaly (RBA) and vertical velocity anomaly profiles to discern daily, weekly, and monthly intensity changes of the DVM pattern using multiple data analysis techniques.

Methods

This research was done as part of the CONsortium for Oil Spill Exposure Pathways in COastal River-Dominated Ecosystems (CONCORDE), an interdisciplinary consortium aimed at

describing oil and dispersant systems transport pathways and organism exposure in the complex shelf region in the river-dominated northern Gulf of Mexico (Greer et al. 2018).

Instrumentation

Acoustic Doppler current profilers

Five upward-facing Teledyne RDI Workhorse four-beam ADCPs were deployed in fixed, 0.5 m high bottom mounts, located ~ 21 km east of the Mississippi River Birdfoot Delta with separation distances of approximately 8 and 12 km in the latitudinal and longitudinal directions, respectively (C1–C5; Fig. 1c; Table 1). The moorings were deployed from 02 November 2015 to 13 April 2016 using the trawl-resistant Barny Sentinel design (Perkins et al. 2000) for protection from the extensive fishing activities in this region. Four ADCPs were 300 kHz measuring continuously every 12 s, whereas the ADCP at C4 was 600 kHz measuring at 1 Hz in hourly bursts of 10 min (see Table 1).

Autonomous underwater glider

A Teledyne Webb Research Slocum autonomous underwater glider, RU31, was deployed on the northern Gulf of Mexico shelf from 13 January 2016 to 12 February 2016. The

glider has typical horizontal and vertical speeds of 20–25 and 10–15 cm s⁻¹, respectively, measuring oceanographic data over the moorings from 02–05 February 2016 with a Sea-bird Scientific conductivity-temperature-depth sensor measuring at 0.5 Hz (see relevant track in Fig. 1c).

Net samples

Plankton samples were collected with a Bedford Institute of Oceanography Net Environmental Sampling System (BIONESS) on 04–05 November 2015 between the surface and at least 2 m above the seafloor at four locations (Fig. 1). Four sets of net samples were collected through 24 h starting at C1 at 8:07 local time (coordinated universal time [UTC] minus 6 h [UTC-h]) on 04 November and ending at C2 at 10:18 (UTC-6) on 05 November. The BIONESS was towed at a speed of 1–1.5 m s⁻¹ and had a 0.25 m² mouth opening fitted with six 333- μ m and three 202- μ m mesh nets. During each BIONESS tow, replicate depth-discrete plankton samples were collected from three approximately equal depth bins representing near-bottom, mid-water, and near-surface strata (three samples per depth bin; nine total samples per BIONESS tow). All samples were preserved in 95% ethanol. Plankton samples were filtered through a 5-mm sieve to remove larger organisms and debris. Subsample portions were sorted, identified into broad taxonomic groupings, and enumerated to estimate total and taxon-specific zooplankton abundances, which were standardized by volume and filtered to yield zooplankton concentration (individuals m⁻³).

Zooplankton in situ imaging and analyses

The In Situ Ichthyoplankton Imaging System (ISIS) was deployed in “tow-yo” fashion during the day and night on 04 November 2015 (UTC-6) in the vicinity of C1 (Fig. 1c). The ISIS uses a shadowgraph lighting technique with a line scan camera (Dalsa, ~ 68 μ m pixel resolution) and a suite of oceanographic sensors to describe the fine-scale distributions of large phytoplankton and zooplankton between ~ 400 μ m and 13 cm (Cowen and Guigand 2008). When towed at speeds of ~ 2.5 m s⁻¹ (at least twice the speed of the nets), it takes ~ 7 s to sample 1 m³ of water, sampling from 1 m below the surface to 2–3 m above the seafloor. The ascent and descent rate of the vehicle was set to 0.2–0.3 m s⁻¹ using motor-actuated wings and onboard software (GreenSea).

Images were processed using a series of steps. Four daytime undulations (9:29–9:49, UTC-6) and four nighttime undulations (21:49–22:13, UTC-6) were chosen. These underwent a flat-fielding procedure to even out the background gray level and remove background artifacts, such as the thin vertical lines produced when using a line scan camera. These flat-fielded images were automatically segmented with image processing software ImageJ (Rasband 2012) by using a threshold gray level value of 170 and extracting particles larger than 1000 pixels (1 mm equivalent spherical diameter; Greer et al. 2017). The size threshold was implemented because smaller particles are difficult to identify and are less likely to vertically migrate and/or produce significant backscatter (Wiebe and

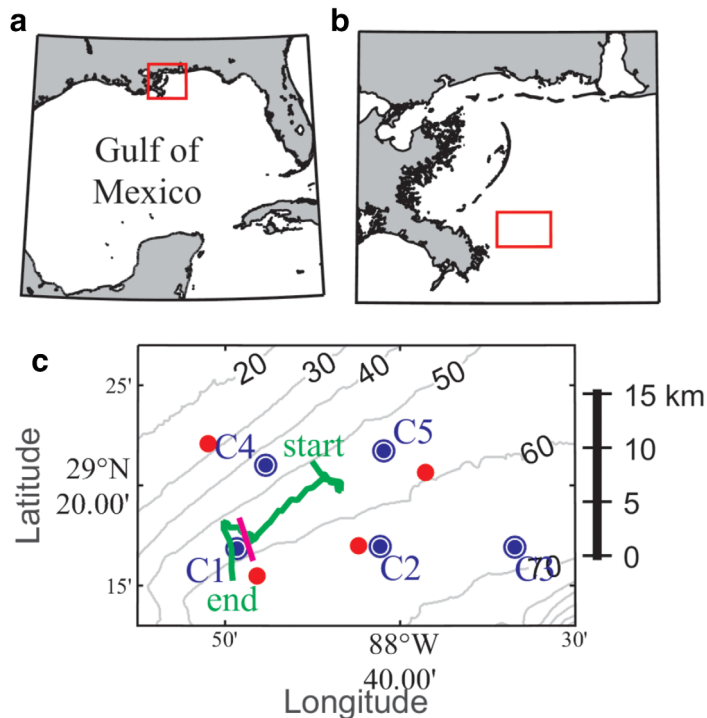


Fig. 1. Map of the study site within the Gulf of Mexico. The red rectangles in (a) and (b) show the location of the Mississippi Bight within the Gulf of Mexico and the study site east of the Mississippi River Birdfoot Delta, respectively. (c) The site was studied using five bottom moorings (blue double circles) and glider data along the green track, with day and night measurements of zooplankton using ISIS tows (straight magenta line near C1) and net tows (red circles). The gray lines represent bathymetric contours every 10 m as labeled. The package M_Map was used to create the maps (<https://www.eoas.ubc.ca/~rich/map.html>).

Table 1. Instrument and measurement details at the five moorings of the ADCPs (Fig. 1c). All times are in UTC.

	C1	C2	C3	C4	C5
Latitude, 29°N	16.85'	16.95'	16.90'	20.10'	21.74'
Longitude, 88°W	49.35'	41.16'	33.45'	47.71'	40.95'
Deployment: November 2015	Third: 00:51	Second: 23:07	Third: 15:59	Third: 02:21	Third: 14:32
Recovery: 13 April 2016	15:58	18:01	19:22	14:19	12:33
Depth (m)	59	65	68	46	56
<i>ADCP measurement settings</i>					
Frequency (kHz)	300	300	300	600	300
Bin size (m)	1	1	1	1.5	1
Top bin depth (m)	4	4	4	5	4
Ping interval (s)	4	4	4	0.5	4
Pings/ensemble	3	3	3	2	3
Ensemble interval (s)	12	12	12	1	12
Burst interval (h)	—	—	—	1	—
Burst duration (min)	—	—	—	10	—

Greene 1994). The resulting 53,487 segments were classified manually into broad taxonomic categories. Only the most common zooplankton (and more likely to produce significant acoustic backscatter) were examined in further analyses.

For elongated taxa, such as chaetognaths and shrimp, an additional processing step was taken to measure their orientation angle. The angle of the major axis of these plankton was automatically extracted in ImageJ. This produced an angle metric where horizontally and vertically oriented zooplankton are represented by angles of 0° and 90°, respectively. Differences in the zooplankton orientation angles between night and day were determined using nonparametric Kruskal–Wallis tests, because the respective orientation variances were unequal. The ISIIS imaging volume is undisturbed and its data have taxon-specific orientation angles for a variety of zooplankton in Monterey Bay, California (Greer et al. 2013), and in the Gulf of Mexico (Greer et al. 2016).

K. brevis detection

A *K. brevis* bloom was tracked into the Mississippi Bight in December 2015 using a satellite remote sensing technique (Soto et al. 2018), indicating high chlorophyll *a* (Chl *a*) and low optical backscatter (Carder and Steward 1985; Mahoney 2003; Cannizzaro et al. 2008). Satellite-derived detection techniques using ocean color imagery have been previously used to detect and track *K. brevis* blooms in the West Florida Shelf validated with data from local agencies (see Soto et al. [2015] for a list and evaluation of this techniques). Ocean color satellite imagery at 1 km pixel resolution from Moderate Resolution Imaging Spectroradiometer (MODIS) onboard the Aqua satellite was obtained from the NASA Goddard Space Flight Center Distributed Active Archive Center. *K. brevis* was detected using the coupled remote sensing reflectance (R_{rs})—fluorescence line height technique. This technique uses two thresholds to identify *K. brevis* blooms: (1) fluorescence line

height above $0.033 \text{ mW cm}^{-2} \mu\text{m}^{-1} \text{ sr}^{-1}$ to detect areas of high Chl *a* and (2) remote sensing reflectance at 555 nm below 0.007 sr^{-1} to detect areas of low optical backscattering properties. The R_{rs} threshold also eliminates pixels with high sediment concentrations, which could generate saturated satellite signals and lead to false *K. brevis* detections. Although there were not enough samples to validate this technique for the area near the moorings, a comparison among detection techniques within a different area that had validation data showed that this methodology performed best (Soto et al. 2015). The statistical evaluation of this technique in the comparison showed 38% false negatives and 5% false positives, meaning that chances of not detecting the bloom are much higher (nearly eight times more likely) than those of detecting a nonbloom.

The MODIS satellite data also provided the daily distributions of cloud cover. Images were categorized as “cloudy” when 100% of the pixels of the study area (area of Fig. 1c, resulting in 1092 pixels of 1 km resolution) had cloud cover (assumed to persist throughout the day). The resulting binary time series consisted of zeros representing “no clouds” days and ones representing “cloudy” days.

Data analysis

ADCP processing

The ADCP profiles were quality controlled to remove inaccurate data (Lu and Lueck 1999; Teledyne 2011). The tests consisted of internal ADCP tests for exclusion of data with poor signal correlation or fish echo signatures (Teledyne 2011), exclusion of ensembles with more than 40% (20% for the usable depth cell nearest to the surface) of the data marked bad by internal checks, and additional correlation and fish echo tests (Book et al. 2007). Echo spikes originating from fish swimming within the ADCP beams contaminate the velocity signal and were removed. However, only ~ 1% of the data

were completely removed by these checks. Data near the bottom and surface were excluded because of standard ADCP acoustic ringing, acoustic surface side lobe contamination, and blanking distance (Teledyne 2011). The height of these excluded regions varied according to the ADCP frequency, bin size, and deployment depth (see Table 1). Therefore, the distance of the uppermost usable depth cell from the surface ranged from 4 to 5 m and the distance from the lowest usable depth cell to the bottom ranged from 2 to 3 m, accounting for the mooring 0.5 m height above the seabed. Data were block averaged every 10 min for the 300 kHz ADCPs (averaging 50 ensembles) and over the 10 min bursts taken every hour for the 600 kHz ADCP at C4 (averaging 600 ensembles; see Table 1 for measurement details). Any remaining data gaps (< 0.02% of the data) were replaced using a linear interpolation of the nearest values in time. Book et al. (2007) provides more details of these processing steps as applied to a similar ADCP dataset. Random error estimates were made for all variables as described in Web Appendix.

Relative backscatter anomaly

The echo intensity profiles averaged across all beams were converted to estimates of relative volume backscattering strength, S_v (relative to a reference backscatter above the ADCP), following Gostiaux and van Haren (2010), a correction of Deines (1999), and then applying a Taylor series expansion of the corrected term as described in Web Appendix. This gives:

$$S_v = A + 10 \log_{10} \left(\frac{R^2}{r_o^2} \right) + 2\alpha R + K_c E_M - \frac{10}{\ln(10)} \frac{N}{S} \quad (1)$$

where S_v is in dB, A is an unknown constant for a given ADCP, R represents the distance to the sample bin (m), r_o is the intensity reference height above the ADCP head (m), α is the sound absorption coefficient of seawater (dB m⁻¹), K_c is the sensitivity coefficient of the ADCP (0.45 dB count⁻¹), E_M is the measured echo intensity by the ADCP (counts), and S/N is the signal (S) to ambient noise (N) ratio. All terms proportional to N^2/S^2 , and higher order have been neglected in this approximation so that the function can be simplified by replacing the complicated logarithmic term in Gostiaux and van Haren (2010) with two linear terms (in logarithmic space) representing the measured echo intensity (fourth term on the right) and the signal to noise ratio (fifth term on the right).

The focus of this work is on the daily variations in the relative backscatter; therefore, a high-pass filter was applied to S_v at each depth bin by means of a fast Fourier transform filter using Hanning windowing with a 36 h cutoff. This quantity will now be referred to as RBA, where positive RBA represents stronger scattering (relative to the mean and low frequency variability) and negative RBA represents weaker scattering. The filtering removes terms that are constant or vary slowly from the backscatter equation, which includes transmitted power,

transmit pulse length, temperature of the transducer, and factors that are constant for a given ADCP as expressed by A . This also includes the spherical spreading term, which is constant, and the attenuation term, which varies slowly with respect to the filter. This filtering process removes possible residual effects, system variability, and unrelated processes that have longer durations than DVMs and primarily leaves only the high-pass filtered data from $K_c E_M$ plus an uncertainty estimate (see Web Appendix). Consequently, the RBA values range from positive to negative, representing high-frequency relative variability from the low-frequency backscatter signal rather than an absolute backscatter.

Vertical swimming velocity

The current velocity calculated by the ADCPs is inferred from the speed of suspended particles using the Doppler shift principle, rather than the water itself (Teledyne 2011). In other words, ADCP measurements of water column currents are based on the key assumption that the average water speed is the average speed of the advected suspended particles (e.g., sediment, biological matter, and bubbles) (Kostaschuk et al. 2005, and references therein). This assumption works well in the case of horizontal velocities measured with suspended particles that include zooplankton because horizontal movements between individual zooplankton are mostly uncorrelated (Heywood 1996; Ott 2005). However, vertical ocean current velocities are generally small (often order mm s⁻¹); therefore, the swimming velocities of zooplankton (often order mm s⁻¹ and larger) can make up a larger fraction of the total vertical movement than of the total horizontal movement of suspended particles (Heywood 1996; Jiang et al. 2007; La et al. 2015). Measured ADCP vertical velocities tend to be lower than vertical swimming speeds of zooplankton because ADCPs average the speeds of all particles, including sediments and non-migrating biological organisms (Plueddemann and Pinkel 1989; Heywood 1996). In our region, even highly horizontally divergent flow (Rossby number order 1) extending over half the water column would produce vertical velocities only of the order of 2 mm s⁻¹. The observed values of the daily patterns of vertical velocities were larger than this throughout the study duration.

As will be shown later, the vertical velocities that were observed have very distinct daily patterns with timing directly associated with dawn and dusk indicating a biological origin. This supports our assumption that measured vertical velocities primarily represent the vertical swimming velocities of zooplankton. Vertical velocities were high-pass filtered in the same way as the RBA and will be referred to as vertical velocity anomalies.

Daily relative backscatter and vertical velocity anomalies patterns

Vertical velocity anomaly and RBA data were reorganized as a function of hour of the day (using a constant time base of UTC-6) and depth, with a window for each day. These RBA and vertical velocity anomaly windows were averaged for each month producing monthly averages of the daily course of

depth variations in these quantities. These were also averaged over the deployment period. Monthly averaging further reduced the vertical velocity anomaly random sampling errors to 0.05–0.1 cm s⁻¹ for the monthly maps and 0.02–0.04 cm s⁻¹ for the overall average maps. The random sampling errors for RBA were reduced to 0.01–0.03 dB (0.16–0.23 dB for C4) for the monthly maps and 0.004–0.015 dB (0.07–0.1 dB for C4) for the overall maps.

Time-augmented empirical orthogonal functions

Daily RBA and vertical velocity anomaly time series were analyzed with an extended, time-augmented empirical orthogonal function (EOF) method. Typical EOF analysis identifies orthogonal combinations (or modes) of time-varying set of records that define new base functions (the modes; Emery and Thomson 2001). The first mode describes the maximum possible variance of the time series that can be described by a single linear combination of the variables. The second mode, when combined with the first mode, explains the maximum variance that can be described by the sum of only two orthogonal combinations, and so on. This analysis can identify particular combinations of records (spatial pattern modes) that covary and explain large percentages of the total temporal variability. An extended time-augmented EOF analysis adds a number of time-lagged or time-advanced versions of the variables into the analysis, which allows the method to describe spatial patterns with set patterns of time evolution. This version of an EOF analysis can be helpful in finding patterns in records with known frequencies of variation like the 24-h patterns of DVMS.

This analysis followed the extended time-augmented EOF method of Book et al. (2016), a modification of the extended EOF method presented by Fraedrich et al. (1993). The RBA and vertical velocity anomaly data were reorganized into daily windows (161 in total), for each particular day for both variables at each mooring. The mean of the 161 daily windows was subtracted from each daily window for both RBA and vertical velocity anomalies before calculating the time-augmented EOFs. The two variables from all five moorings were concatenated into one inclusive matrix for the EOF analysis of 161 d by 24 h by number of depth bins for all moorings. Then, an extended time-augmented EOF analysis was performed to find set patterns of the daily window variability over the longer time-periods of the mooring deployment. For example, instead of needing 161 (number of complete deployment days) of these windows per mooring to describe the complete time series variation of daily RBA patterns, only three windows (i.e., modes) per mooring and their time amplitude values can be used to describe 50% of the time series variance of daily RBA and vertical velocity anomaly patterns. Results show dominant modes of variability in the RBA and vertical velocity anomaly profiles at all the moorings.

To validate the EOF results, the propagation of the errors in the vertical velocity anomalies and RBA through the EOF calculations were quantified using a bootstrap method with 100 error ensembles. For the 300 kHz ADCPs, modes 1 through 3 have

backscatter uncertainty errors less than 0.06, 0.09, and 0.12 dB, respectively. For the 600 kHz ADCP at C4, RBA uncertainty errors in modes 1 through 3 were less than 0.36, 0.54, and 0.72 dB, respectively. At all the ADCPs, vertical velocity uncertainty errors in modes 1 through 3 were less than 0.03, 0.04, and 0.05 cm s⁻¹, respectively. Estimated uncertainty errors in the temporal amplitudes of the three EOF modes were all below 0.001. These error analysis results strongly support the validity of the EOF results in describing the main patterns of DVM that were occurring during this study.

Wavelet coherence

A wavelet coherence analysis was used to describe the relationship between depth-averaged currents and RBA variations. Wavelet coherence allows for the comparison between two non-stationary time series by calculating localized correlation coefficients in time-frequency space (Torrence and Compo 1998; Grinsted et al. 2004). Regions of statistically significant coherence were calculated using the Monte Carlo method (Grinsted et al. 2004).

Results

Relative backscatter and vertical velocity anomalies

Monthly averages of daily RBA at all the moorings displayed a pattern that changed abruptly at dawn and dusk, with lower values in daytime than nighttime and decoupled from the physical oceanography, suggesting a biological origin (Fig. 2). The daily ranges of RBA varied throughout the nearly 6-month deployment, with minimum daily RBA ranges occurring in late fall (< 5 dB difference between day and night) and maximum daily RBA ranges occurring in spring (> 10 dB difference between day and night). The ranges of diel RBA varied slightly between the different locations, with the shallower ones (C1 and C5) having larger day-to-night ranges (~ 12 dB) than deeper ones (~ 8 dB at C2 and C3), except at C4 (~ 6 dB) likely because of the different ADCP acoustic frequency at that location.

The monthly averaged RBA change was disproportionately stronger at dawn (> 5 dB) relative to dusk (< 3 dB), especially at moorings C1, C2, and C5. A downward movement in maximum RBA is clearly observed a few hours before sunrise. As the maximum RBA moved downward, a region of lower RBA developed near the surface (e.g., see C1 in January, top 20 m, hours before sunrise) in some cases. This could represent a decrease in scatterers in the upper 20 m as they migrated downward. The maximum RBA at dusk did not display as clear a trend of vertical migration. On the contrary, RBA sometimes appeared to also move downward at dusk (e.g., see C3 in February in Fig. 2), while lacking a clear strong maximum like the one seen at dawn. Likewise to the predawn near-surface lower RBA, a region of lower RBA near the bottom also appeared just after dusk (e.g., see C1 and C5 in March below 40 m in Fig. 2) in some cases. This suggests that the increase in RBA at night might originate from above with downward migrators. The dramatic changes in RBA at dawn/dusk occurred nearly simultaneously

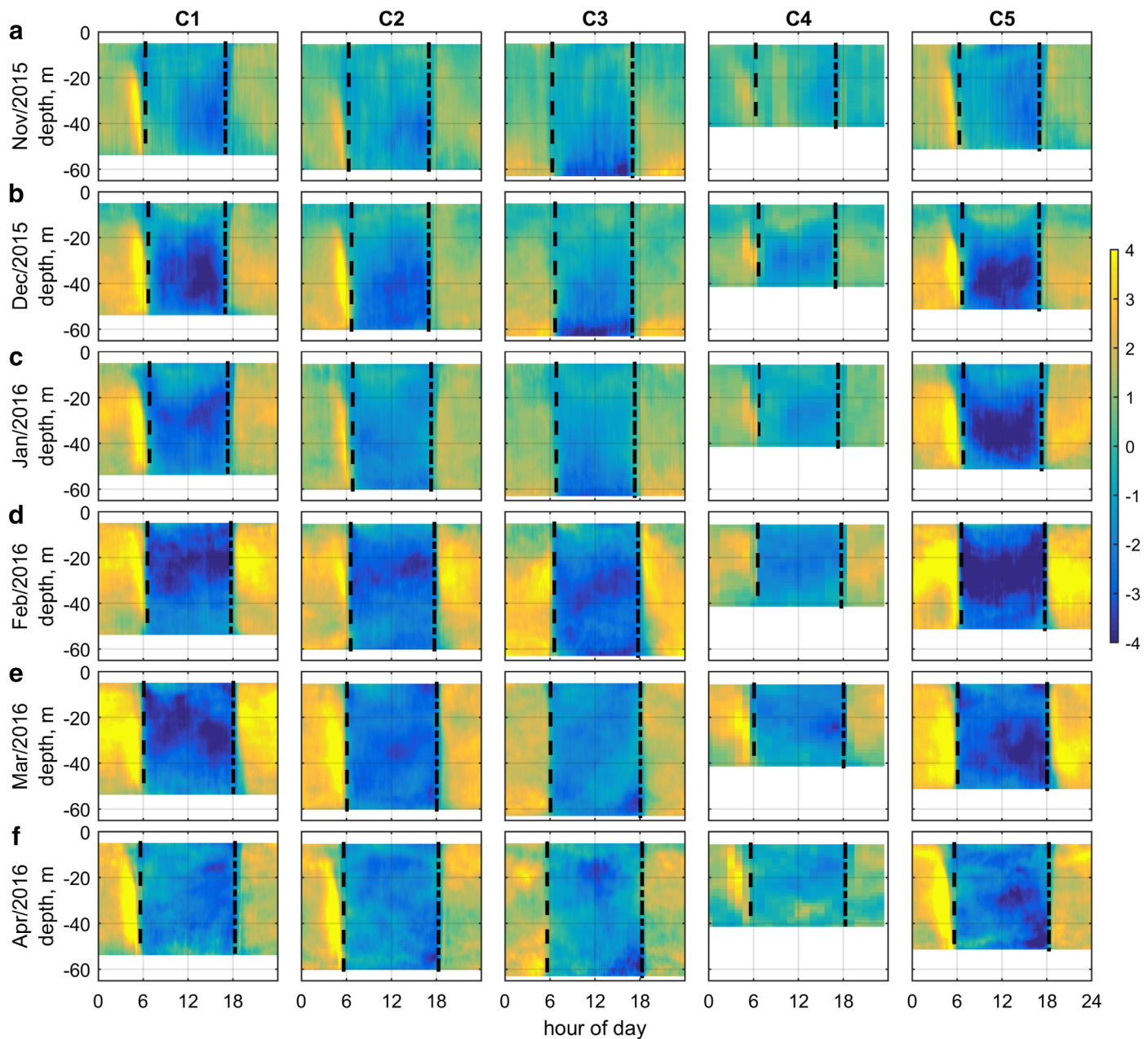


Fig. 2. Monthly mean of RBA plotted as a function of hour of day in UTC-6 and depth. Each row represents a different month: (a) November 2015, (b) December 2015, (c) January 2016, (d) February 2016, (e) March 2016, and (f) April 2016, and each column is a different mooring. Dashed line represents sunrise, and dash-dot line denotes sunset.

at all the moorings (Fig. 3), demonstrating a wide spatial coverage for the vertical migration.

A daily pattern was also found in the vertical velocity anomalies that changed direction at dawn and dusk, with daytime upward (positive) and nighttime downward (negative) movement (Fig. 4). Upward velocities (positive in red contours) were generally found near the surface at around sunrise and around sunset. These upward velocities were generally concurrent with lower RBA values, suggesting either lower zooplankton scattering or abundance than those moving downward. Upward velocities

at sunrise were strongest in March 2016 (Fig. 4d,e). Consistent downward velocities were observed before dawn, coinciding with the downward movement of positive RBA. The strongest downward velocities ($< -0.6 \text{ cm s}^{-1}$) were observed soon after dusk in April (Fig. 4f) following strong upward velocities ($> 0.3 \text{ cm s}^{-1}$) observed at sunset.

Plankton taxa, orientations, and interactions

Zooplankton were identified with net samples and the ISIS imagery during both day and night. The limited number of

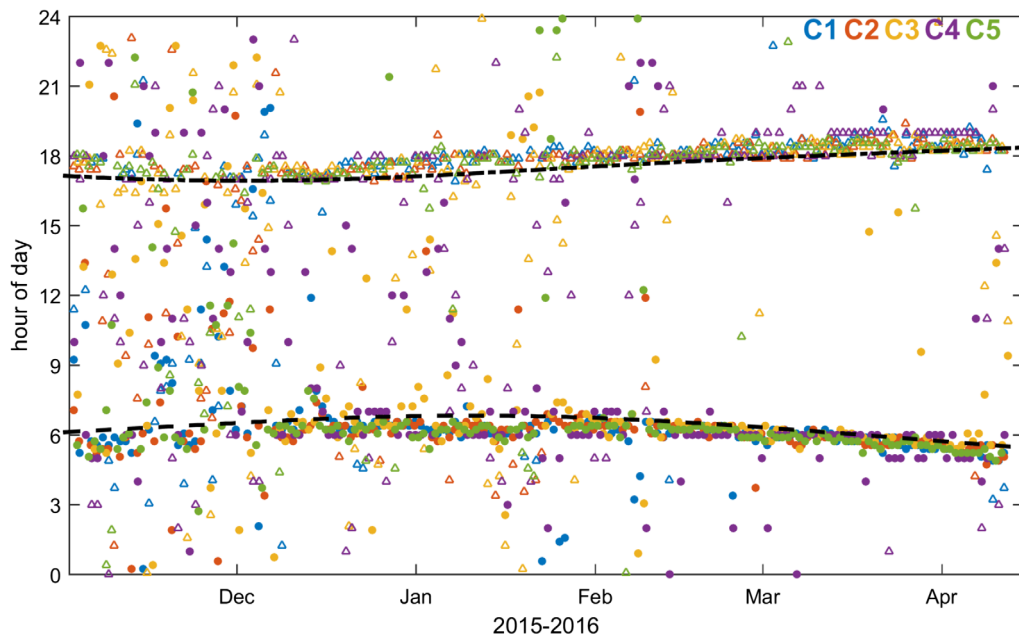


Fig. 3. Times of daily maximum changes in depth-averaged RBA. Hollow triangles represent maximum increase and filled circles represent maximum decrease in RBA, with colors representing each mooring. The dashed line represents sunrise, whereas the dash-dot line represents sunset. The hours of day in the y -axis are in UTC-6.

samples with the plankton nets prevent any statistical analysis of DVM patterns; however, they do provide information on the identity of potential scatterers. The most common zooplankton taxa captured in the net samples were ostracods, copepods, and chaetognaths (Fig. 5). The zooplankton were dispersed throughout the water column in most of the profiles, except at C2, where ostracods (Fig. 5a) and, to a lesser extent, copepods (Fig. 5b) were predominantly found near the bottom.

The ISIS also characterized zooplankton taxa and concentrations in the water column but at a much higher vertical resolution than nets. Given a minimum size of 1 mm equivalent spherical diameter for ISIS image processing, the most common zooplankton were hydromedusae, shrimp, and chaetognaths (Fig. 6a). The two most abundant zooplankton were chaetognaths and hydromedusae, both displaying nocturnal DVM behavior. Chaetognaths were between 2 and 15 times more abundant than hydromedusae or shrimp except close to the surface (outside the ADCP vertical range), where shrimp dominated during the day and hydromedusae were more common at night (Fig. 6b). Chaetognath abundances ranged from 8 to 37 individuals m^{-3} . They were generally dispersed below 7 m in daytime and at higher concentrations relative to nighttime. The nighttime chaetognath distribution was skewed toward increasing concentrations toward the surface, except for a drop in concentration in the most near-surface measurements. Hydromedusae abundances ranged from 0 to 13 individuals m^{-3} , with similar distributions as chaetognaths but lacking the decrease in near-surface nighttime concentrations. Shrimp abundances ranged from 0 to 18 individuals m^{-3} and displayed characteristics of a reverse DVM pattern, aggregating in a thin

layer within the shallowest 3 m in daytime (out of the ADCPs' range) with abundances of up to 18 individuals m^{-3} and dispersing throughout the water column at night.

In addition to zooplankton abundances, the ISIS images were further processed to measure particle orientations (Fig. 6c). Both shrimp and chaetognaths were more likely to orient near-vertically during the day (Kruskal-Wallis, $p < 8 \times 10^{-8}$ for shrimp and $p < 2 \times 10^{-16}$ for chaetognaths). For chaetognaths, their nighttime orientations were significantly more variable (F -test, $p < 2 \times 10^{-16}$) than their daytime orientations. The majority of daytime surface-dwelling shrimp within the thin layer were oriented vertically ($> 60^\circ$), whereas at night, shrimp displayed no preferred angle of orientation.

Satellite imagery indicated the presence of *K. brevis* in the northeastern shelf of the Gulf of Mexico during autumn 2015 (Soto et al. 2018). This 2015 *K. brevis* bloom was tracked with validation from local agencies, showing the succession of the bloom from the Florida Panhandle in October toward the Mississippi Bight through December. The HAB was inferred to move over the moorings in mid-December 2015 (Fig. 7a,b), when the DVM signal in the RBA strengthened (Fig. 7c). The highest inferred *K. brevis* abundance over the moorings was on 15 December and decreased considerably by 19 December (Fig. 7a,b). During 14–20 December, the RBA signal above ~ 20 m showed weak changes between day and night (~ 2 dB range) while it varied considerably below 20 m (~ 16 dB range; Fig. 7c).

DVM spatiotemporal variations

The mean RBA structure, as represented by mooring C1, showed higher nighttime values throughout the water column

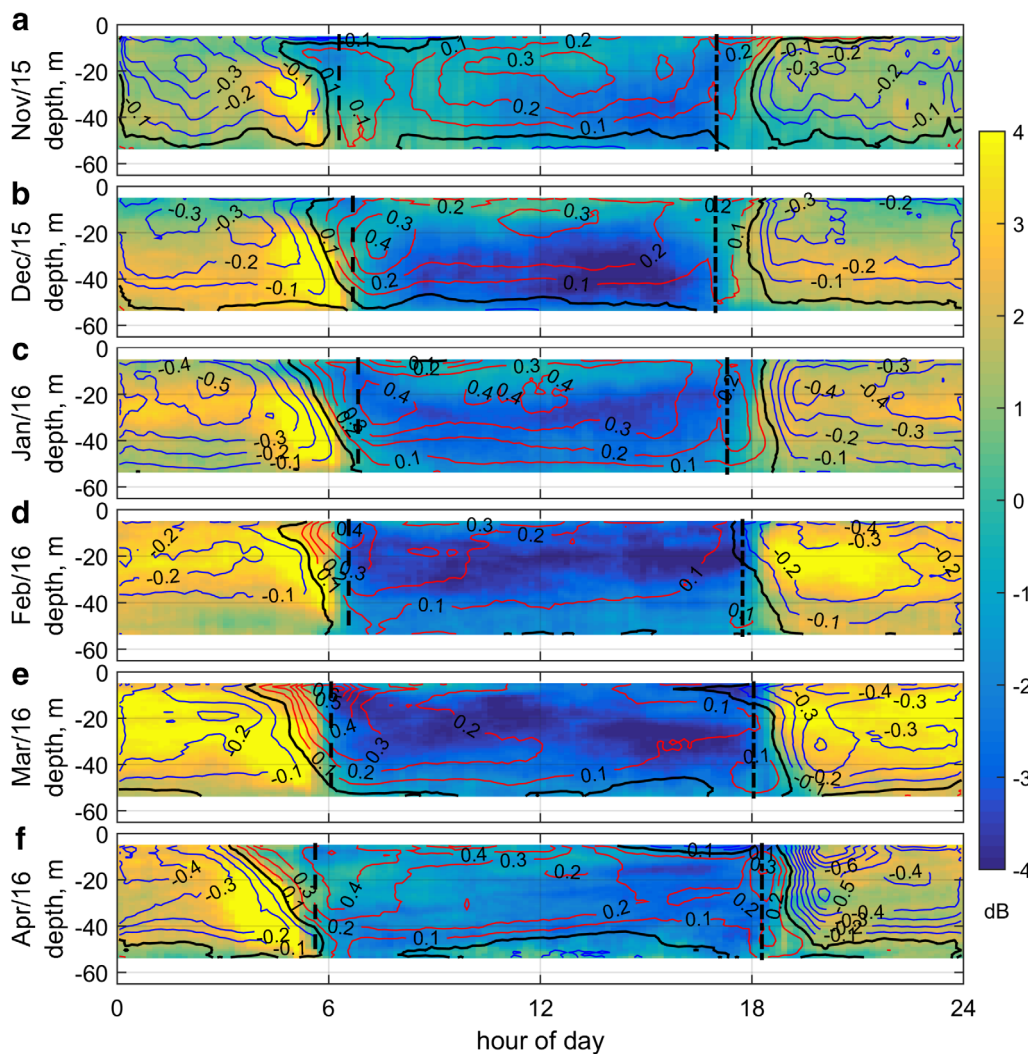


Fig. 4. Monthly mean of the RBA (filled contours, same as the first column of Fig. 2) overlain by the vertical velocity anomalies (contour lines; cm s^{-1}) at C1 plotted as a function of hour of day in UTC-6 and depth. The red contour lines represent positive vertical velocity anomalies, black is zero, and blues are negative. The dashed line represents sunrise, whereas the dash-dot line represents sunset. Each row represents a different month: (a) November 2015, (b) December 2015, (c) January 2016, (d) February 2016, (e) March 2016, and (f) April 2016 with the average sunrise (dashed) and sunset (dot dash) times for each.

(Fig. 8a). The mean vertical velocity anomaly structure presented downward velocities (down to -0.4 cm s^{-1}) concentrated in the upper three fourths of the water column at night and upward velocities ($\sim 0.1 \text{ cm s}^{-1}$) in daytime that were strongest near dawn.

The EOF analysis of relative backscatter and vertical velocity anomalies revealed three different dominant components of the diel patterns, which accounted for 34%, 16%, and 10% of the total variability (Fig. 8b–d). The mode patterns were consistent between all the moorings; therefore, only the modes at C1 are presented for simplicity and clarity. The EOF modes represent anomalies from a mean field, and, therefore, Fig. 9 is used to show the total relative backscatter and vertical velocity anomalies patterns that would result from each mode's maximum and minimum realized amplitudes.

Mode 1: Interseasonal variability and shelf transport

The structure of mode 1 (Fig. 8b) resembled the mean RBA pattern (Fig. 8a). Positive temporal amplitudes of mode 1 represent a strengthening of the mean RBA pattern (Fig. 9b), such as the stronger DVM signals observed in February and March (Fig. 2e). Conversely, negative mode 1 amplitudes represent a weakening of the mean RBA signal (Figs. 8b, 9c), such as the weaker signals in November (Fig. 2a). Mode 1 also displayed a slightly positive linear trend during the 6-month deployment, generally displaying more frequent negative temporal amplitudes in November and December and more frequent positive amplitudes in February and March.

Positive mode 1 amplitudes also represent a strengthening of the upward velocities (up to 1 cm s^{-1}) at dawn and downward ($< -0.6 \text{ cm s}^{-1}$) at dusk (Figs. 8b, 9b), especially near the

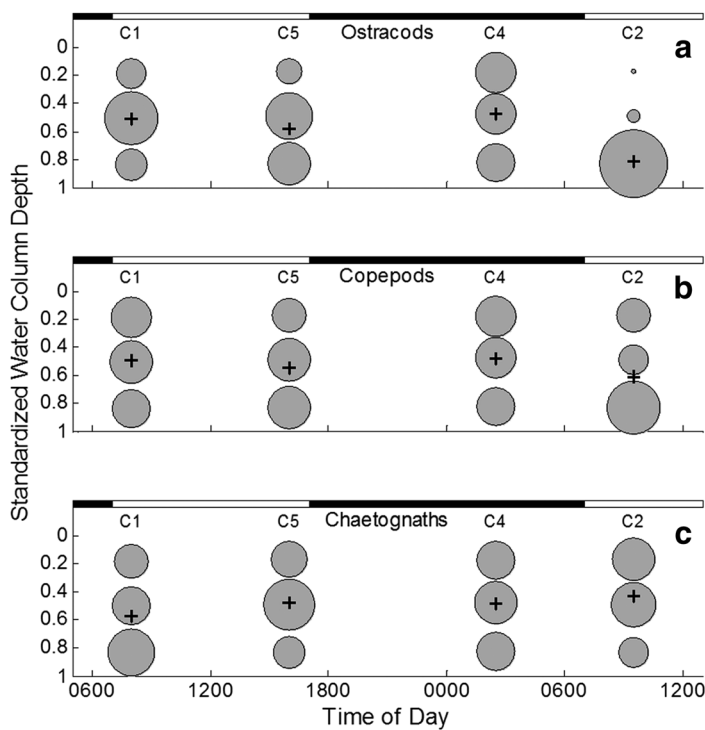


Fig. 5. Zooplankton results from net samples. Mean depth of occurrence (+) and concentration-weighted proportions at depth (gray filled circles) for (a) ostracods, (b) copepods, and (c) chaetognaths collected near the four array stations (C1, C5, C4, and C2; see Fig. 1c for actual collection sites). Mean depth of occurrence was calculated for each taxon following Brodeur and Rugen (1994). Each location was sampled near surface, mid-depth, and near bottom. Relative proportions of zooplankton at depth were standardized by taxon concentration. Depth is standardized by the maximum depth for each station for comparison among stations, where 0 = surface and 1 = maximum depth sampled. Time of day is in UTC-6 on 04–05 November 2015. The dark bars above the figure denote night periods; the white bars denote day periods.

surface (top 10–20 m). The strong upward velocities after dawn were concentrated toward the surface, coinciding with low RBA (Fig. 9b). This pattern could match a reverse DVM pattern, where scatterers might migrate to above the ADCPs detection range (< 5 m) during the day and migrate downward at night (similar to the shrimp measured with the ISIS). Negative mode 1 amplitudes represent weakened upward velocities, especially around dawn (Fig. 9b), which matches the corresponding weakening and near disappearance of the RBA DVM signal. However, downward vertical velocity anomalies at night remain relatively unchanged from the mean regardless of the amplitude of mode 1 (Fig. 9a–c).

In addition to the positive linear trend throughout the deployment, DVM signal intensity also appeared to modulate with shelf transport direction. The orientation of the standard deviation ellipses (Wong and Lee 2005, see section 5.3.2) shows that shelf currents, while relatively weak in their means, had high levels of variability (up to 0.7 m s^{-1}) concentrated in a single principal direction axis at each site (Fig. 10a). A wavelet coherence analysis between mode 1 amplitudes and

the principal component of the currents at C1 (currents oriented along the ellipse major axis) showed an inverse relationship at periods of 16–32 d (vectors pointing left meaning 180° out of phase; Fig. 10b). This inverse relationship suggests lower DVM intensity with northeastward currents (directed toward the Mississippi coast) and higher DVM intensity with southwestward currents (directed offshore).

This relationship with the current direction has implications with respect to the Mississippi River plume. Northeastward currents could transport the Mississippi River plume over the moorings. For example, the presence of the freshwater plume at the surface near C1 in February could have limited the vertical extent of the DVMs, as observed by the shortened high backscatter band at dawn on 04 February relative to 03 February (Fig. 11). In other words, the deepening and intensifying halocline after sunset on 03 February could have confined the higher RBA region at dawn on 04 February to depths below the halocline (~ 15 m) instead of to its usual shallower starting depth (as seen on 03 February). However, higher RBA was also observed above the halocline at around 23:00 of 03 February, a pattern not found at 23:00 on 04 February. Therefore, the presence of the Mississippi River plume could have different effects on the DVM patterns of different organisms, where some may not extend into the plume while others appear within it.

Mode 2: Depth dependent distribution of migrators

In contrast to the mean and mode 1, mode 2 RBA spatial pattern represents the vertical movement of a relatively narrow depth band of high RBA (Fig. 8c). A positive mode 2 amplitude presents high nighttime RBA only in the bottom half of the water column and the appearance of high daytime RBA near the top third of the water column, which suggests a reverse DVM pattern (Fig. 9d). However, the vertical velocity anomalies were more varied than the RBA. The high RBA at sunrise coincided with negative velocities that point to nocturnal DVM, while the high RBA at sunset also coincided with negative velocities suggesting reverse DVM (Figs. 8c, 9d). Upward velocities were strongest at dawn and near the surface in daytime (Fig. 9d). The strongest positive mode 2 peak occurred in early and mid-December.

Negative mode 2 amplitudes slightly strengthened and added depth structure to the mean DVM pattern, producing higher intensities at night and lower during the day (Fig. 9e), except in the bottom 20 m. Negative mode 2 amplitudes dampened vertical velocity anomalies throughout. The strongest negative amplitude peaks occurred in mid-February and early March (Fig. 8e). Positive mode 2 amplitude peaks were more common in winter, while negative mode 2 peaks were more common in spring.

Mode 3: Lunar phase

Positive mode 3 amplitudes represent an amplification of the downward RBA movement at dawn (Fig. 8d) together with strengthened downward vertical velocity anomalies (Fig. 9f). Negative mode 3 amplitudes, therefore, weaken or negate the

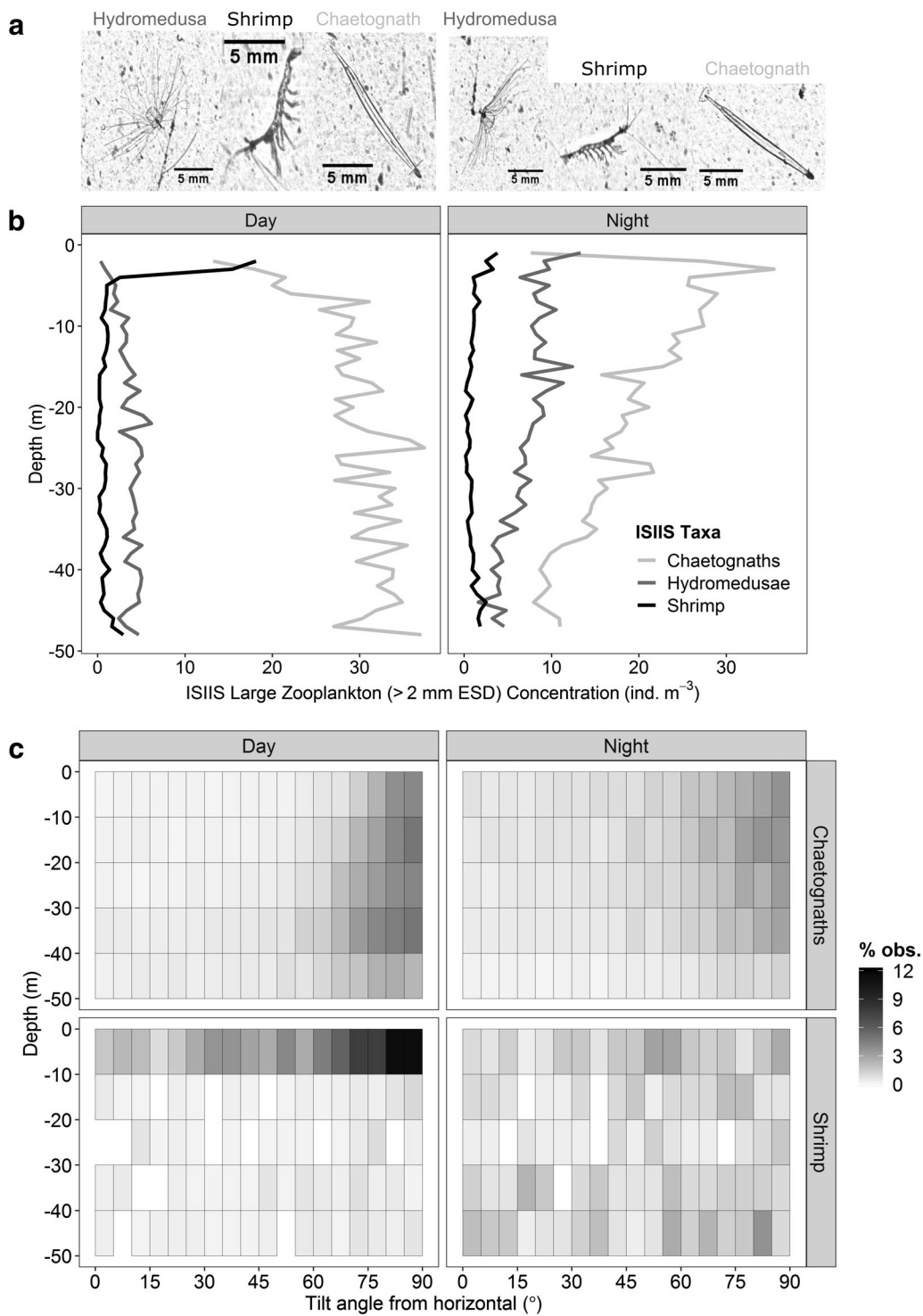


Fig. 6. Observations of hydromedusa, shrimp, and chaetognath zooplankton with the ISIS on 04 November 2015. **(a)** Images with actual orientations captured during both day and night. **(b)** Average vertical distribution of zooplankton at 1 m vertical resolution for both day and night. **(c)** Percentage of observations of chaetognaths and shrimp at different depths and tilt angle from horizontal in degrees (i.e., orientation angle). The sum of percentages for each of the four panels adds up to 100%. Orientation angles represent vertical orientation as 90° and horizontal as 0°, relative to the bottom. Blank spots represent zero observations at that depth and angle combination.

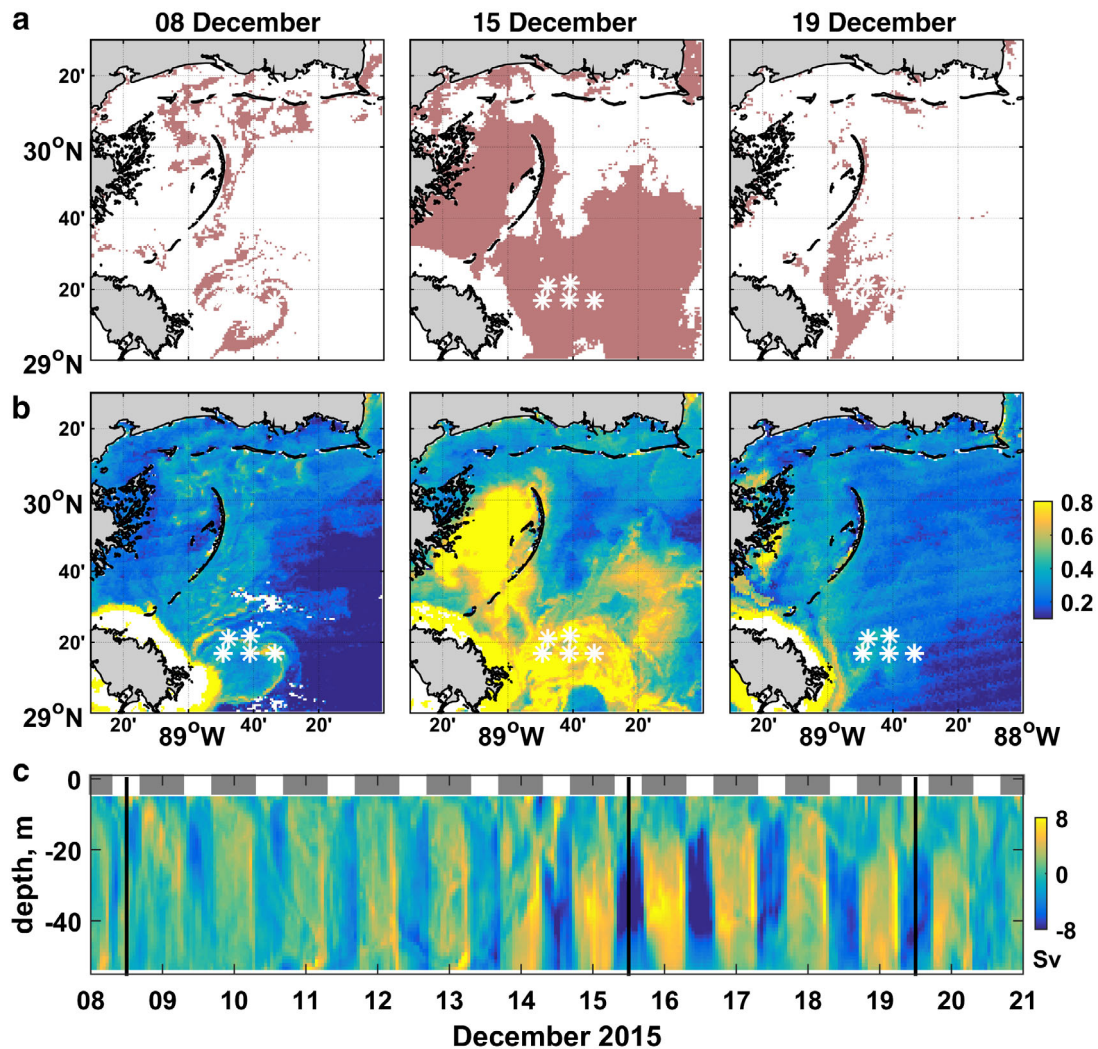


Fig. 7. *K. brevis* maps of (a) HAB detection where pink represents likely HAB regions and (b) normalized fluorescence line height for 08, 15, and 19 December 2015, where yellow and blue represent highest and lowest surface values, respectively, and white represents areas without values. The asterisks show the mooring locations. (c) RBA at C1 with daily gray overhead bars representing nighttime. The bold black lines represent the three instances of the maps above set at noon UTC-6.

downward movement of high RBA at dawn (Fig. 9g). Mode 3 amplitudes oscillated about zero throughout the deployment with a period of around a month, which inversely correlated to the lunar phase ($r = -0.47$, $p < 1 \times 10^{-7}$; Fig. 10c). This relationship suggests that a new moon results in stronger sunrise downward migration.

Discussion

The deployment of multiple high-resolution sensors can compensate for the shortcomings of each, which include but are not limited to spatial, taxonomic, or temporal resolutions. The multisensor sampling approach used in this study could be deployed for long-term ecosystem monitoring of zooplankton populations (and DVMs) and the utility of the moored acoustic

system increases when community compositions and orientation behaviors are better described in the sampling area.

Scatterers

Zooplankton species were sampled with net tows and the ISIIS throughout the water column during both day and night in early November 2015. Discrepancies between nets and ISIIS results could be attributed to different factors. Nets do not sample hydromedusae and other gelatinous species quantitatively because most are destroyed by extrusion through the net mesh (Warren et al. 2001; Remsen et al. 2004). The ISIIS analysis presented here did not consider particles smaller than 1 mm equivalent spherical diameter because of processing limitations. Also, particles smaller than 1 mm were dominated by detritus, which likely would not produce as strong of an acoustic backscatter signal, nor is it capable of performing

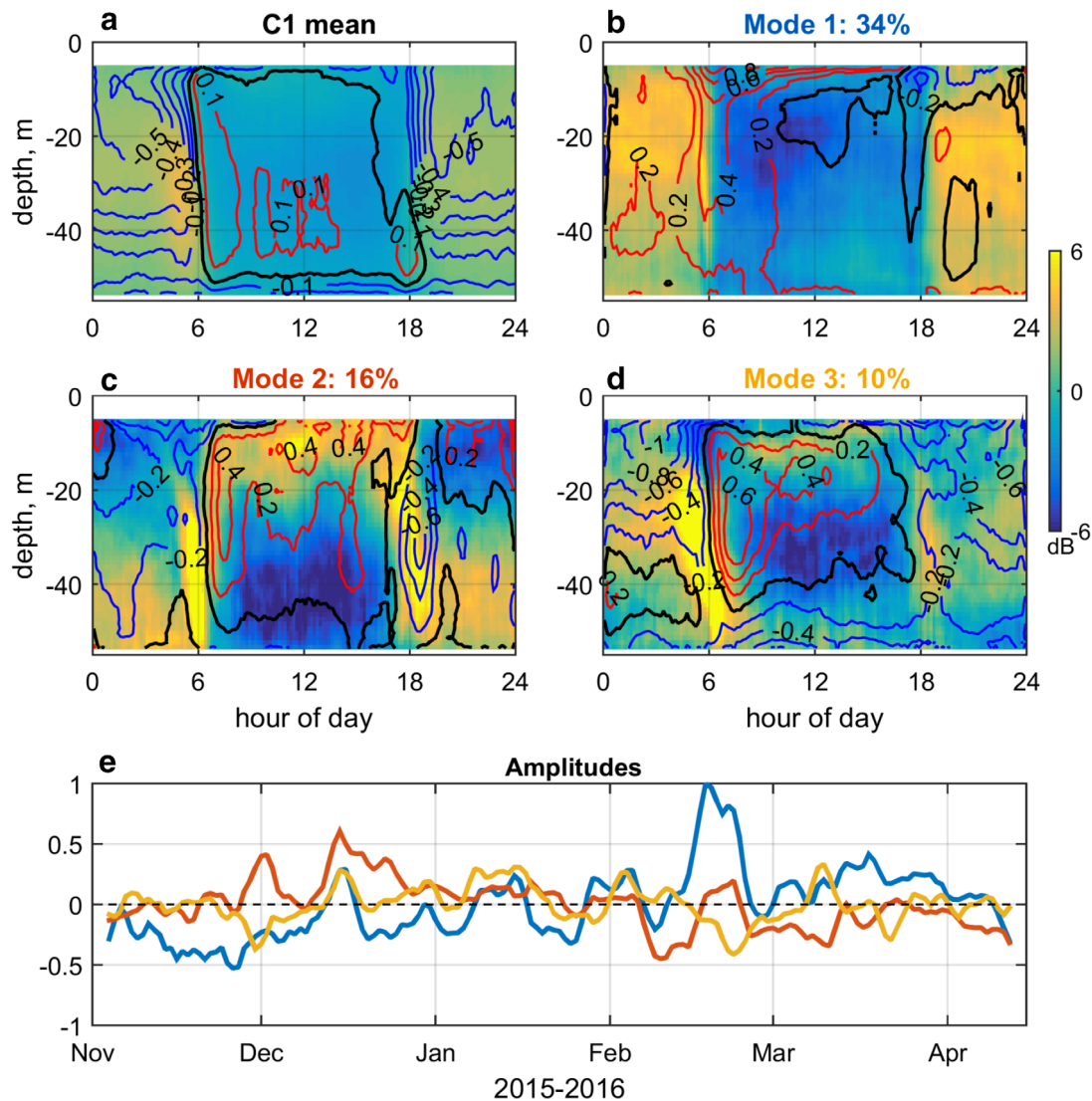


Fig. 8. Time-augmented EOF analysis results for C1 (representative of the other mooring locations). (a) The 24 h temporal patterns of the mean RBA (filled contours) and vertical velocity anomalies (contour lines, cm s^{-1}) as a function of hour of the day in UTC-6 and depth, followed by the daily structure of the first three EOF modes (b-d). For the vertical velocity anomaly contours, red represents positive values, black is zero, and blue represents negative values, as labeled. (e) The temporal amplitudes of the three EOF modes, where blue is mode 1, orange is mode 2, and yellow is mode 3.

daily vertical migrations. Furthermore, the ISIS is towed at nearly twice the speed of the nets, allowing for the sampling of faster zooplankton that likely contribute substantially to acoustic backscatter. A direct comparison between bongo nets and the ISIS revealed that the ISIS sampled larger larval fishes compared to the net system (Cowen et al. 2013).

When considering spherical scatterers (e.g., sediment), ADCPs have a range of scatterer diameters and material properties that reflect acoustic energy efficiently for the ADCP's acoustic frequency band. For ADCPs of 300 and 600 kHz, the particle diameters that produce the strongest backscatter are around 1.25 and 0.63 mm, respectively (Emery and Thomson 2001, p. 93). Stanton and Chu (2000) found that shape and material properties such as particle roughness and material

composition heterogeneities play a significant role in the scattering. It is beyond the scope of the present study to delve into the relationships between different scatterers and backscattering value. However, the 300 kHz ADCPs used in this study (all but one site) should be sensitive to scatterers of about the same size as those measured by the ISIS and, therefore, can provide family or genus-level identifications of the dominant scatterers in the ADCP data.

From our two biological sampling methods, copepods, chaetognaths, and shrimp appear to be the most likely scatterers because of their abundance. Although large jellies (10s of cm bell diameter) have been demonstrated to produce acoustic backscatter (e.g., Mutlu 1996; Brierley et al. 2005; De Robertis and Taylor 2014), hydromedusae of the size found in

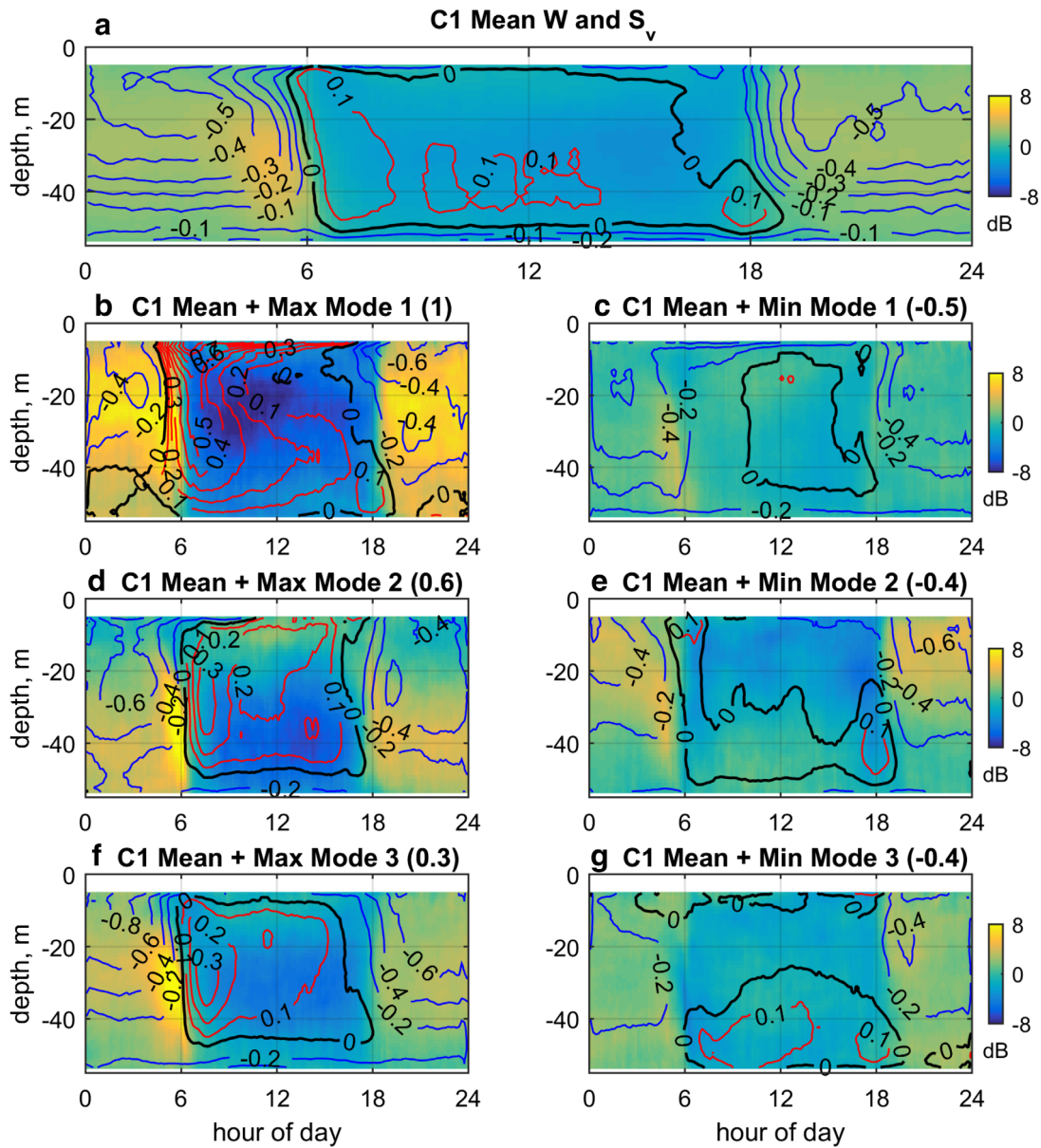


Fig. 9. Contours of RBA and vertical velocity anomaly at C1. (a) Mean RBA contours (filled) with overlaying contour lines of vertical velocity anomaly. Summation of the mean with the (b, d, f) maximum and (c, e, g) minimum temporal amplitudes (modes 1–3) for both RBA and vertical velocity anomalies. The filled contours (with color unit ranges on the right) represent RBA. The contour lines (red for positive, black for zero, and blue for negative) represent the contours of vertical velocity anomalies (cm s^{-1}). The numbers in parentheses for each subtitle represent the temporal amplitude of that mode used in the plot. Hours are in UTC-6.

our study (1–2 cm bell diameter) likely do not produce significant acoustic backscattering in the concentrations found at our sites. Shrimp showed the clearest signal of a DVM pattern in the ISIIS data, performing reverse DVMs and concentrating in the shallowest 3 m during the day (outside the range of the ADCPs), then spreading out over the water column at night. Yet, acoustics are sometimes difficult to interpret when mixed assemblages of zooplankton are present because of different acoustic impedance properties and behaviors among individuals (Lavery et al. 2007). Biological sampling was only done at

the start of the mooring deployment; consequently, other organisms could have been important scatterers during other times of the deployment. Further sampling of this area is needed to describe seasonal changes in zooplankton composition, and this would also help with the ecological interpretation of this dataset.

Day and night backscatter intensity changes

The diel backscatter shows a clear pattern of lower daytime values throughout the water column relative to nighttime.

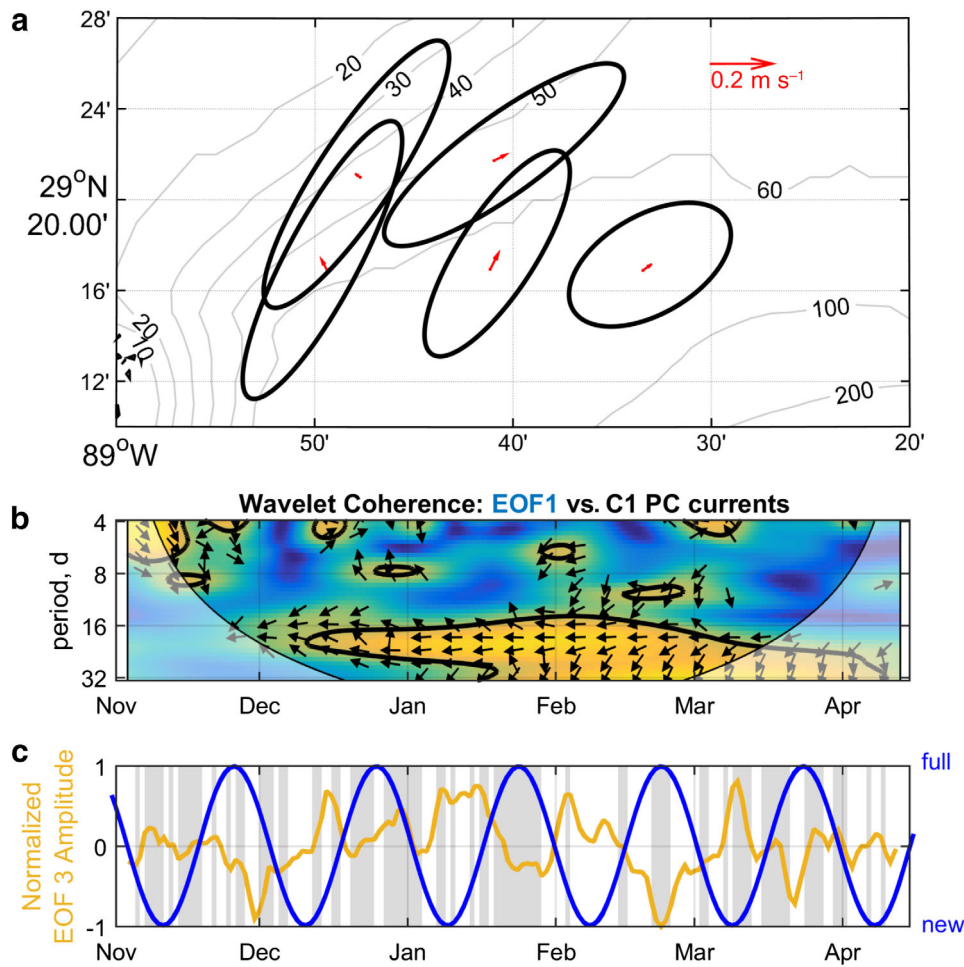


Fig. 10. (a) Standard deviation ellipses (black) and mean vectors (red) of depth-averaged currents at all moorings. Gray contours represent bathymetric isobaths as numbered. (b) Wavelet coherence between the time-augmented EOF mode 1 and the principal component of the depth-averaged currents at C1 (~ 32° clockwise from north). The bold black contour represents the 95% significance level. Phase vectors show in phase pointing right and out of phase pointing left. The grayed region is the cone of influence where values are less reliable because of edge effects. (c) Time series of the normalized time-augmented EOF mode 3 amplitudes (yellow) and the lunar phase (blue), where 1 and -1 represent the full and new moon, respectively. The gray areas represent days with cloud cover, as determined from satellite imagery.

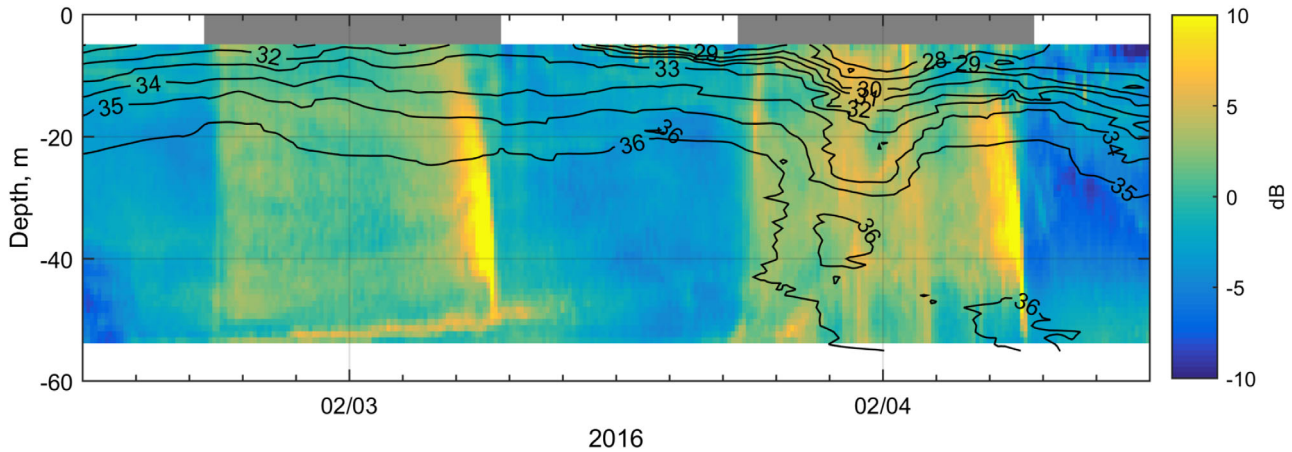


Fig. 11. RBA is represented by the filled contours at C1, and salinity (psu) is represented with the labeled black contours from the glider near C1 (see Fig. 1 for glider track). Time is in UTC-6. Daily gray overhead bars represent nighttime.

The stark diel differences could be attributed to multiple, potentially additive causes such as: (1) horizontal advection of scatterers by daily local circulation (e.g., tides and inertial currents), (2) diel horizontal migration of scatterers, (3) movement of scatterers outside the ADCP's vertical range of observations (either to the surface or bottom), (4) changes in organism concentration and vertical swimming speed vertical gradients, or (5) changes in the in situ orientation of the scatterers (i.e., tilt angle) between day and night. The observed vertical velocity anomaly patterns are complex and do not generally agree with either a simple nocturnal DVM or a simple reverse DVM pattern. These factors are further discussed below.

Daily advection of scatterers

Advection of scatterers was observed in the analysis, where on- or off-shelf circulation resulted in decreased or increased RBA intensity, respectively. However, the circulation variability was on the order of days to weeks. The RBA signal showed repeated sharp backscatter changes (within hours) throughout the water column at nearly every sunrise and sunset (Fig. 3). Possible daily circulation patterns include inertial, tidal, or land-sea breeze forced currents (all near 24-h cycle in this area). The observed daily horizontal currents (from a combination of tides, inertia, and land-sea breeze) in this region did not occur in phase with sunset and sunrise (results not shown). Furthermore, these near-daily horizontal currents did not dominate the total observed horizontal currents (accounting for 5–10% of the variability) and could not have caused the strong and consistent daily RBA changes.

Diel horizontal migrations

Changes in RBA at dawn and dusk occurred simultaneously at all sites, which makes diel horizontal migrations unlikely (Fig. 3). Although diel horizontal migration has been described in areas with strong bathymetric slopes or habitat gradients (e.g., Benoit-Bird et al. 2001), these findings may be less applicable to our study site, which has a weak bathymetric slope and homogenous sandy bottom habitat. In other words, horizontally migrating organisms near the mooring array (with distances of 5–10 km between moorings) likely would not gain a fitness advantage that is often implicated as a driver of animal migrations (e.g., Pearre 2003).

Scatterers beyond ADCP range

A likely contributor to the diel RBA signal is the movement of scatterers beyond the ADCP's vertical range of observation. The backscatter profiles presented here do not include the top ~ 4 m nor the bottom ~ 3 m (i.e., ~ 10% of the water column), while the ISIS and net measurements also missed the bottom ~ 2 to 3 m. High-resolution ISIS measurements found shrimp aggregating near the shallowest 3 m in daytime. Near-bottom aggregations of ostracods and cumaceans have been found to perform nocturnal DVM by remaining in the benthos during the day and swimming to the surface at night (Macquart-Moulin 1999; Cohen and Forward 2009). The

daytime movement of migrators like shrimp to the surface and other species to the bottom would result in greatly reduced daytime RBA intensity. For example, high RBA intensity moved toward the bottom and disappeared just before sunrise as represented by the slanting RBA contour lines (Fig. 9a,b,d,f). A similarly strong RBA at dusk is not generally observed, suggesting a more gradual ascent at dusk, which would result in lower RBA relative to the descent at dawn. The stronger dawn RBA suggests a concerted decent in response to sunrise.

Organism concentration and vertical swimming speed vertical gradients

Any estimation of the downward movement of RBA should consider vertical gradients in both organism concentration and vertical swimming speed. For example, the simple case of a vertical clustering of migrators moving upward or downward at a constant speed will cause the associated RBA clustering to likewise move. Conversely, vertical changes in swimming speed within a vertically uniform distribution of migrators will also cause migrators to bunch up or disperse and create vertical movement of RBA clusters.

Zooplankton orientation

Another factor that likely enhanced the daily RBA variations was the diel change in zooplankton orientation angle. Results showed near vertically oriented chaetognaths and shrimp in daytime and more random orientations at night. Vertically oriented, elongate zooplankton, such as chaetognaths and shrimp, present a smaller cross-sectional area relative to horizontally oriented elongated zooplankton, if observed from below by an ADCP. Theoretical results from Stanton and Chu (2000) showed that changes in orientation angle, as observed by acoustic frequencies of 200 and 420 kHz, caused target strength variability for copepods of 10–20 dB and for euphausiids of 20–30 dB (see figs. 5 and 6 in Stanton and Chu [2000]). Our observed day to night differences of 300 kHz RBA was 2–15 dB, which is well within the dB changes estimated by Stanton and Chu (2000) that could be completely explained by only zooplankton orientation changes.

Elongate larval fishes have been shown to perform similar vertical orientation behavior during daytime hours (Greer et al. 2016). Diel orientation differences have also been observed by Benfield et al. (2000) in Georges Bank with the Video Plankton Recorder. Another nighttime survey found a near-instantaneous change in backscatter (by up to 15 dB) by turning a deck light on and off due to changes in plankton orientation (Trevorrow et al. 2005). The difference in orientation preference between day and night would change the backscatter intensity even with no change in zooplankton abundance or vertical distribution. This fact could explain a portion of the diel RBA changes found in this study. Little is known about the drivers of variation in zooplankton orientation. Better descriptions of the drivers of orientation behavior are needed to improve the accuracy of abundance estimates

derived from acoustic backscatter. For example, abundance estimates derived from backscatter proxies for elongated zooplankton that exhibit this orientation behavior would be biased either high or low depending on what time of day the biological calibration measurements were performed to derive the proxies.

The presented zooplankton orientation angles are meaningful. Multiple lines of evidence suggest that there is negligible turbulence generated from the vehicle itself, considering the imaging area is at the front and offset from the tow point by 1.5 m, which minimizes disturbances at the image.

The first comes from this study. Turbulence from the sampler (if present) would not change between day and night, and this would result in random orientation angles for both day and nighttime tows, which was not the case. There are also published studies showing dramatic differences in orientation among organisms with similar sizes and morphological characteristics (Greer et al. 2013, 2016). In Monterey Bay, using almost the exact same system as for the present study, Greer et al. (2013) demonstrated that two ctenophores species with different feeding behaviors displayed orientations within the image as would be predicted. The lobate ctenophore (an ambush predator) oriented vertically and a *Pleurobrachia* spp. ctenophore, which swims in a spiral to collect zooplankton on its tentacles, had a more random orientation. These orientation differences could not have been detected if the vehicle generated substantial turbulence.

Interseasonal variability

This nearly 6 month ADCP dataset allowed for the study of DVM variability between late autumn and spring. The DVM daily ranges in RBA were lowest in late autumn increasing considerably toward spring, as evident in the positive linear trend of mode 1 amplitudes. This is consistent with previous studies of DVMs. For example, a year-long study of ADCP moorings throughout the southwestern Gulf of Mexico by Ochoa et al. (2013) observed stronger DVM backscatter in the longer summer days when compared to the shorter winter days. Another study by Jiang et al. (2007) near Bermuda in the Atlantic Ocean showed a clear seasonal cycle in DVM, with more intense DVM signals in spring than in winter using ADCP data. The present study was the first to examine interseasonal zooplankton DVM dynamics on the continental shelf of the northern Gulf of Mexico.

Lunar variability

In addition to interseasonal variability, DVMs varied with the lunar cycle. Mode 3 separated the lunar variability from the main signal. An inverse relationship was found between mode 3 and the lunar phase, suggesting stronger downward migrations at sunrise during the new moon. This relationship is mainly driven by the changes in nighttime light intensity between new and full moons because light levels are an important driver of DVMs (Prihartato et al. 2016; Aksnes et al. 2017).

Studies have found relationships between the lunar cycle and DVM intensity as observed in the backscatter, in the Gulf

of Mexico (Ochoa et al. 2013) and Canary Island waters (Hernández-León et al. 2010). They suggest an alternative hypothesis that lunar variability increased predation by interzonal diel vertical migrants during new moons, where a decrease in predation during full moons allowed zooplankton to increase in abundance.

In our study, the lunar pattern appeared to be modulated by cloud cover, with more cloud cover during full moons yielding a stronger migration signal in the RBA at sunrise relative to a full moon with clear skies. This finding is similar to previous works showing an increase in diel signal in the RBA in response to cloud cover observed in backscatter from an ADCP (Pinot and Jansá 2001) and in lobster larvae (Rimmer and Phillips 1979), although these studies did not consider lunar phasing.

Largest mode 1 event

The largest EOF event was observed in mode 1 during the second half of February and lasted approximately 10–15 d. The driving forces for this record event were difficult to explain. Three possibilities emerged as factors in its development: a prolonged period of weak currents and winds, waxing moon, and an extended period of cloudless days (Fig. 10c). This peak occurred between two cold front wind events on 09 and 25 February (not shown), which generated relatively weak wind and current velocities. This time period also encompassed a waxing moon phase (from new to full moon) as the peak progressed, suggesting a potential lunar effect. The third possible factor was that the month of February experienced the greatest number of cloudless days of the entire deployment. A combination of these factors could strengthen the observed mode 1 patterns during that time. Further research could clarify the occurrence and development of such DVM strengthening.

Circulation-driven dynamics

Circulation patterns coupled with water mass origin and DVM behavior influenced the RBA daily intensity. Shelf currents were related to mode 1, where southwestward currents (advecting productive shelf waters offshore) were associated with stronger DVMs (more intense daily RBA ranges) compared to northeastward currents (onshore transport of oligotrophic waters below nutrient-rich Mississippi River plume waters; Fig. 10). Circulation analysis of the currents showed they were primarily modulated by the wind (Greer et al. 2018). For example, southeastward winds lower the water level along the Louisiana coast (set-down). The resulting coastal low pressure produces northeastward currents in response to the geostrophic balance between this pressure gradient and the Coriolis acceleration. For northwestward winds, the reverse is true where a setup of water (increase of water level) against the coast drives southwestward currents in response. These southwestward currents would carry highly productive waters from the Mississippi Bight over the moorings. Sindlinger et al. (2005) observed increased DVM backscatter intensities along the off-shelf 1000 m isobath in the northeastern Gulf of Mexico (east and

south of the Mississippi River Birdfoot Delta), that were correlated with currents oriented away from the shelf from both the Mississippi Bight and Mississippi River. In our case, on the shelf, we further distinguish a difference in DVM amplification from these two distinct sources.

The Mississippi River plume was detected over the moorings in early February with glider profiles (Fig. 11) that showed the plume deepening from a few meters to ~ 15 m near C1 throughout 03 February 2016. The RBA from C1 suggests that a deepening plume acted as a barrier for some migrating zooplankton, as observed by the difference in vertical extent of high RBA just before sunrise between 03 and 04 February. The relatively strong halocline could have inhibited migration between the layers for at least some zooplankton species (Graham et al. 2001). However, relatively high RBA was also found within the plume at around 23:00 h of 03 February, which was not present 1 d earlier when the plume was shallower. These observations suggest that zooplankton vertical migrations change in response to the presence of river plumes and stratification in various ways. Longer concurrent time series of salinity, backscatter, and sampling with higher taxonomic resolution (e.g., in situ imaging) are needed to help elucidate the environmental factors influencing these zooplankton behaviors.

The likely presence of a near-surface *K. brevis* HAB that made its way to the moorings in December driven by along-shelf currents (Soto et al. 2018) appeared to strengthen DVMs in mid-December (Fig. 7a,b), most clearly seen as a positive peak in mode 2 amplitudes (Figs. 8e, 9d). The strongest DVM during the bloom presented sharp daily RBA changes below 15 m of up to 16 dB (Figs. 7c, 9d). Previous studies found *K. brevis* performing reverse DVMs in the northern Gulf of Mexico shelf, where they remained within the top 2 m during the day and migrated down to 10 m (in 20–40 m deep waters) at night (Hu et al. 2016; Qi et al. 2017). Although the observed enhancement of DVMs were too deep (> 15 m) to be directly attributed to *K. brevis*, it is possible that the presence of the toxic *K. brevis* bloom modified the behavior of zooplankton, producing the changes in intensity and structure of the DVMs (EOF modes 1, 2, and 3 amplitudes all have local peaks). Possible causes include predator/grazer avoidance, increased grazing, or behavioral changes caused by toxicity. Some zooplankton have been observed feeding on *K. brevis* regardless of its toxicity (Turner and Tester 1989; Hansen et al. 1998; Cohen et al. 2007; Hong et al. 2012), while others have reduced abundances during *K. brevis* blooms (Lester et al. 2008).

Implications

Zooplankton vertical migrations can affect pollutant exposure rates as well as oceanographic processes. Vertical migrations could greatly increase their vulnerability to pollutants such as oil advected at different depths (Graham et al. 2010; Buskey et al. 2016; Daly et al. 2016); therefore, it is important to understand how planktonic distributions are modulated

under different oceanographic conditions. The DVM patterns described in this study may have a direct link to the magnitude of environmental impacts from a future contamination event.

Conclusion

Relative backscatter and vertical velocity anomalies were measured by moored ADCPs for nearly 6 months on the southwestern shelf of the Mississippi Bight. The data show a remarkably consistent and strong pattern of daily changes associated with zooplankton, with an abrupt 2–15 dB change in RBA between daytime and nighttime. Strong RBA at night was associated with relatively stronger downward vertical velocity anomalies (0.1–0.5 cm s⁻¹) and weak RBA during the day was associated with relatively weaker upward vertical velocity anomalies (0.1 cm s⁻¹).

A time-augmented EOF analysis showed that 34% of the variability of these patterns was primarily due to strengthening or weakening of the intensity of the mean pattern rather than to changes in the mean pattern structure. Strengthening of the pattern was found to be correlated with currents bringing waters from the coastal shelf of the Mississippi Bight, whereas weakening was correlated with currents bringing waters from offshore and from the Mississippi River plume. The second most common pattern accounted for 16% of the variability and was primarily due to the addition of depth structure to the mean patterns with a peak of this mode occurring during the presence of a *K. brevis* HAB in mid-December. An additional 10% of the variability of the mean pattern was primarily due to changes in the time structure of the pattern within its 24 h cycle, particularly close to dawn. This third mode of variability was found to be associated with the lunar cycle and the amount of daily cloud cover.

Net and ISIIS observations suggest the most likely acoustically observed migrating zooplankton were chaetognaths, shrimp, copepods, and ostracods, although with seasonal changes in the zooplankton community, other groups likely contributed to acoustic backscatter during the study period. Shrimp displayed a clear reverse DVM pattern. The basic repeating pattern of abrupt changes in RBA from night to day over the entire water column observed by the ADCPs could be explained by three patterns: (1) migrators moving to the near-surface region beyond the valid range of ADCP measurements (as in the reverse DVM observed in shrimp), (2) migrators moving to the near-bottom region beyond the valid range of ADCP measurements (nocturnal DVM), and (3) orientation changes in elongated zooplankton from random at night to near-vertical during the day (not necessarily associated with any migration). Chaetognaths and shrimp showed a strong preference for vertical orientation during the day. However, it is unlikely that orientation changes alone were solely responsible for all the diel patterns that were observed given the complex patterns of RBA and vertical velocity anomaly

variability that were found in this dataset. The combination of high spatiotemporal resolution acoustic data with net and in situ imaging provided a unique opportunity to observe inter-seasonal (fall through spring) zooplankton DVM on the biologically productive northern Gulf of Mexico shelf. Further observations are needed in this dynamic region to fully understand the strong and complex DVM patterns that this first study has revealed.

References

- Aksnes, D. L., A. Røstad, S. Kaartvedt, U. Martinez, C. M. Duarte, and X. Irigoien. 2017. Light penetration structures the deep acoustic scattering layers in the global ocean. *Sci. Adv.* **3**: e1602468. doi:10.1126/sciadv.1602468
- Barth, L. E., W. G. Sprules, M. Wells, and M. Coman. 2014. Seasonal changes in the diel vertical migration of *Chaoborus punctipennis* larval instars. *Can. J. Fish. Aquat. Sci.* **71**: 665–674. doi:10.1139/cjfas-2013-0440
- Benfield, M. C., C. S. Davis, and S. M. Gallager. 2000. Estimating the in-situ orientation of *Calanus finmarchicus* on Georges Bank using the video plankton recorder. *Plankt. Biol. Ecol.* **47**: 69–72.
- Benoit-Bird, K. J., W. W. L. Au, R. E. Brainard, and M. O. Lammers. 2001. Diel horizontal migration of the Hawaiian mesopelagic boundary community observed acoustically. *Mar. Ecol. Prog. Ser.* **217**: 1–14. doi:10.3354/meps217001
- Benoit-Bird, K. J., and G. L. Lawson. 2016. Ecological insights from pelagic habitats acquired using active acoustic techniques. *Annu. Rev. Mar. Sci.* **8**: 463–490. doi:10.1146/annurev-marine-122414-034001
- Book, J. W., H. Perkins, R. P. Signell, and M. Wimbush. 2007. The Adriatic circulation experiment winter 2002/2003 mooring data report: A case study in ADCP data processing. Memorandum report NRL/MR/7330-07-8999. Naval Research Laboratory.
- Book, J. W., and others. 2016. Propagation of internal tides on the northwest Australian shelf studied with time-augmented empirical orthogonal functions, p. 744. *In* The Proceedings of the 20th Australasian Fluid Mechanics Conference. *Australian Fluid Mechanics Society*; [accessed 2018 June 1]. Available from <https://people.eng.unimelb.edu.au/imarusic/proceedings/20/744Paper.pdf>.
- Brewer, G. D., and G. S. Kleppel. 1986. Diel vertical distribution of fish larvae and their prey in nearshore waters of southern California. *Mar. Ecol. Prog. Ser.* **27**: 217–226. doi:10.3354/meps027217
- Brierley, A. S. 2014. Diel vertical migration. *Curr. Biol.* **24**: R1074–R1076. doi:10.1016/j.cub.2014.08.054
- Brierley, A. S., D. C. Boyer, B. E. Axelsen, C. P. Lynam, C. A. J. Sparks, H. J. Boyer, and M. J. Gibbons. 2005. Towards the acoustic estimation of jellyfish abundance. *Mar. Ecol. Prog. Ser.* **295**: 105–111. doi:10.3354/meps295105
- Brodeur, R. D., and W. C. Ruge. 1994. Diel vertical distribution of ichthyoplankton in the northern Gulf of Alaska. *Fish. Bull.* **92**: 223–235. doi:10.1016/j.marenvres.2012.06.009
- Buskey, E. J., H. K. White, and A. J. Esbaugh. 2016. Impact of oil spills on marine life in the Gulf of Mexico: Effects on plankton, nekton, and deep-sea benthos. *Oceanography* **29**: 174–181. doi:10.5670/oceanog.2016.81
- Cannizzaro, J. P., K. L. Carder, F. R. Chen, C. A. Heil, and G. A. Vargo. 2008. A novel technique for detection of the toxic dinoflagellate, *Karenia brevis*, in the Gulf of Mexico from remotely sensed ocean color data. *Cont. Shelf Res.* **28**: 137–158. doi:10.1016/j.csr.2004.04.007
- Carder, K. L., and R. G. Steward. 1985. A remote-sensing reflectance model of a red-tide dinoflagellate off West Florida. *Limnol. Oceanogr.* **30**: 286–298. doi:10.4319/lo.1985.30.2.0286
- Cohen, J. H., P. A. Tester, and R. B. Forward. 2007. Sublethal effects of the toxic dinoflagellate *Karenia brevis* on marine copepod behavior. *J. Plankton Res.* **29**: 301–315. doi:10.1093/plankt/fbm016
- Cohen, J. H., and R. B. Forward. 2009. Zooplankton diel vertical migration—a review of proximate control, p. 77–110. *In* R. Gibson, R. Atkinson, and J. Gordon [eds.], *Oceanography and marine biology: An annual review*. Taylor & Francis.
- Comyns, B. H., and J. Lyczkowski-Shultz. 2004. Diel vertical distribution of Atlantic croaker, *Micropogonias undulatus*, larvae in the northcentral Gulf of Mexico with comparisons to red drum, *Sciaenops ocellatus*. *Bull. Mar. Sci.* **74**: 69–80.
- Cowen, R. K., and C. M. Guigand. 2008. In situ ichthyoplankton imaging system (ISIIS): System design and preliminary results. *Limnol. Oceanogr. Methods* **6**: 126–132. doi:10.4319/lom.2008.6.126
- Cowen, R. K., A. T. Greer, C. M. Guigand, J. A. Hare, D. E. Richardson, and H. J. Walsh. 2013. Evaluation of the in situ ichthyoplankton imaging system (ISIIS): Comparison with the traditional (bongo net) sampler. *Fish. Bull.* **111**: 1–12. doi:10.7755/FB.111.1.1
- Daly, K. L., U. Passow, J. Chanton, and D. Hollander. 2016. Assessing the impacts of oil-associated marine snow formation and sedimentation during and after the Deepwater horizon oil spill. *Anthropocene* **13**: 18–33. doi:10.1016/j.ancene.2016.01.006, doi: 10.1016/j.ancene.2016.01.006
- De Robertis, A., and K. Taylor. 2014. In situ target strength measurements of the scyphomedusa *Chrysaora melanaster*. *Fish. Res.* **153**: 18–23. doi:10.1016/j.fishres.2014.01.002
- Deines, K. L. 1999. Backscatter estimation using broadband acoustic Doppler current profilers. *Proceedings of the IEEE Sixth Working Conference on Current Measurement*. IEEE. 249–253.
- Dzwonkowski, B., K. Park, H. K. Ha, W. M. Graham, F. J. Hernandez, and S. P. Powers. 2011. Hydrographic variability on a coastal shelf directly influenced by estuarine outflow. *Cont. Shelf Res.* **31**: 939–950. doi:10.1016/j.csr.2011.03.001
- Dzwonkowski, B., and others. 2017. Estuarine influence on biogeochemical properties of the Alabama shelf during the

- fall season. *Cont. Shelf Res.* **140**: 96–109. doi:[10.1016/j.csr.2017.05.001](https://doi.org/10.1016/j.csr.2017.05.001)
- Emery, W. J., and R. E. Thomson. 2001. *Data analysis methods in physical oceanography*, 1st ed. Elsevier. doi:[10.1016/B978-0-444-50756-3.X5000-X](https://doi.org/10.1016/B978-0-444-50756-3.X5000-X)
- Farmer, D. M., and H. J. Freeland. 1983. The physical oceanography of fjords. *Prog. Oceanogr.* **12**: 194219–194219. doi:[10.1016/0079-6611\(83\)90004-6](https://doi.org/10.1016/0079-6611(83)90004-6)
- Fraedrich, K., S. Pawson, and R. Wang. 1993. An EOF analysis of the vertical-time delay structure of the quasi-biennial oscillation. *J. Atmos. Sci.* **50**: 3357–3365. doi:[10.1175/1520-0469\(1993\)050<3357:AEAOTV>2.0.CO;2](https://doi.org/10.1175/1520-0469(1993)050<3357:AEAOTV>2.0.CO;2)
- Gilliam, J. F., and D. F. Fraser. 1987. Habitat selection under predation hazard: Test of a model with foraging minnows. *Ecology* **68**: 1856–1862. doi:[10.2307/1939877](https://doi.org/10.2307/1939877)
- Gostiaux, L., and H. van Haren. 2010. Extracting meaningful information from uncalibrated backscattered echo intensity data. *J. Atmos. Ocean. Technol.* **27**: 943–949. doi:[10.1175/2009JTECHO704.1](https://doi.org/10.1175/2009JTECHO704.1)
- Graham, W. M., F. Pagès, and W. M. Hamner. 2001. A physical context for gelatinous zooplankton aggregations: A review, p. 199–212. *In* *Jellyfish blooms: Ecological and societal importance*. Springer Netherlands. doi:[10.1007/978-94-010-0722-1_16](https://doi.org/10.1007/978-94-010-0722-1_16)
- Graham, W. M., R. H. Condon, R. H. Carmichael, I. D'Ambra, H. K. Patterson, L. J. Linn, and F. J. Hernandez Jr. 2010. Oil carbon entered the coastal planktonic food web during the Deepwater Horizon oil spill. *Environ. Res. Lett.* **5**: 45301. doi:[10.1088/1748-9326/5/4/045301](https://doi.org/10.1088/1748-9326/5/4/045301)
- Greer, A. T., R. K. Cowen, C. M. Guigand, M. A. McManus, J. C. Sevadjan, and A. H. V. Timmerman. 2013. Relationships between phytoplankton thin layers and the fine-scale vertical distributions of two trophic levels of zooplankton. *J. Plankton Res.* **35**: 939–956. doi:[10.1093/plankt/fbt056](https://doi.org/10.1093/plankt/fbt056)
- Greer, A. T., C. Briseño-Avena, A. L. Deary, R. K. Cowen, F. J. Hernandez, and W. M. Graham. 2017. Associations between lobster phyllosoma and gelatinous zooplankton in relation to oceanographic properties in the northern Gulf of Mexico. *Fish. Oceanogr.* **26**: 693–704. doi:[10.1111/fog.12228](https://doi.org/10.1111/fog.12228)
- Greer, A. T., C. B. Woodson, C. M. Guigand, and R. K. Cowen. 2016. Larval fishes utilize Batesian mimicry as a survival strategy in the plankton. *Mar. Ecol. Prog. Ser.* **551**: 1–12. doi:[10.3354/meps11751](https://doi.org/10.3354/meps11751)
- Greer, A. T., and others. 2018. Functioning of coastal river-dominated ecosystems and implications for oil spill response: From observations to mechanisms and models. *Oceanography* **31**: 90–103. doi:[10.5670/oceanog.2018.302](https://doi.org/10.5670/oceanog.2018.302)
- Griffiths, G., and J. I. Diaz. 1996. Comparison of acoustic backscatter measurements from a ship-mounted Acoustic Doppler Current Profiler and an EK500 scientific echosounder. *ICES J. Mar. Sci.* **53**: 487–491. doi:[10.1006/jmsc.1996.0070](https://doi.org/10.1006/jmsc.1996.0070)
- Grinsted, A., J. C. Moore, and S. Jevrejeva. 2004. Application of the cross wavelet transform and wavelet coherence to geophysical time series. *Nonlinear Process. Geophys.* **11**: 561–566. doi:[10.5194/npg-11-561-2004](https://doi.org/10.5194/npg-11-561-2004), 5/6
- Hamner, W. M. 1995. Predation, cover, and convergent evolution in epipelagic oceans. *Mar. Freshw. Behav. Physiol.* **26**: 71–89. doi:[10.1080/10236249509378930](https://doi.org/10.1080/10236249509378930)
- Hansen, P. J., P. A. Tester, and J. T. Turner. 1998. Interactions between toxic marine phytoplankton and metazoan and protistan grazers, p. 453–473. *In* D. M. Anderson, A. D. Cembella, and G. M. Hallegraeff [eds.], *NATO SGI*. Springer.
- Hays, G. C. 2003. A review of the adaptive significance and ecosystem consequences of zooplankton diel vertical migrations, p. 163–170. *In* M. B. Jones, A. Ingólfsson, E. Ólafsson, G. V. Helgason, K. Gunnarsson, and J. Svavarsson [eds.], *Migrations and dispersal of marine organisms*. Springer. doi:[10.1007/978-94-017-2276-6_18](https://doi.org/10.1007/978-94-017-2276-6_18)
- Heath, M. R., E. W. Henderson, and D. L. Baird. 1988. Vertical distribution of herring larvae in relation to physical mixing and illumination. *Mar. Ecol. Prog. Ser.* **47**: 211–228. doi:[10.3354/meps047211](https://doi.org/10.3354/meps047211)
- Heil, C. A., D. A. Bronk, M. R. Mulholland, J. M. O'Neil, P. W. Bernhardt, S. Murasko, J. A. Havens, and G. A. Vargo. 2014. Influence of daylight surface aggregation behavior on nutrient cycling during a *Karenia brevis* (Davis) G. Hansen & Ø. Moestrup bloom: Migration to the surface as a nutrient acquisition strategy. *Harmful Algae* **38**: 86–94. doi:[10.1016/j.hal.2014.06.001](https://doi.org/10.1016/j.hal.2014.06.001)
- Hernández-León, S., G. Franchy, M. Moyano, I. Menéndez, C. Schmoker, and S. Putzeys. 2010. Carbon sequestration and zooplankton lunar cycles: Could we be missing a major component of the biological pump? *Limnol. Oceanogr.* **55**: 2503–2512. doi:[10.4319/lo.2010.55.6.2503](https://doi.org/10.4319/lo.2010.55.6.2503)
- Heywood, K. J. 1996. Diel vertical migration of zooplankton in the Northeast Atlantic. *J. Plankton Res.* **18**: 163–184. doi:[10.1093/plankt/18.2.163](https://doi.org/10.1093/plankt/18.2.163)
- Holt, G. J., and S. A. Holt. 2000. Vertical distribution and the role of physical processes in the feeding dynamics of two larval sciaenids *Sciaenops ocellatus* and *Cynoscion nebulosus*. *Mar. Ecol. Prog. Ser.* **193**: 181–190. doi:[10.3354/meps193181](https://doi.org/10.3354/meps193181)
- Hong, J., S. Talapatra, J. Katz, P. A. Tester, R. J. Waggett, and A. R. Place. 2012. Algal toxins alter copepod feeding behavior. *PLoS One* **7**: e36845. doi:[10.1371/journal.pone.0036845](https://doi.org/10.1371/journal.pone.0036845)
- Hu, C., B. B. Barnes, L. Qi, C. Lembke, and D. English. 2016. Vertical migration of *Karenia brevis* in the northeastern Gulf of Mexico observed from glider measurements. *Harmful Algae* **58**: 59–65. doi:[10.1016/j.hal.2016.07.005](https://doi.org/10.1016/j.hal.2016.07.005)
- Hutchinson, G. E. 1967. *A treatise on limnology, introduction to lake biology and the limnoplankton*. John Wiley and Sons. doi:[10.4319/lo.1969.14.3.0472](https://doi.org/10.4319/lo.1969.14.3.0472)
- Jiang, S., T. D. Dickey, D. K. Steinberg, and L. P. Madin. 2007. Temporal variability of zooplankton biomass from ADCP backscatter time series data at the Bermuda Testbed Mooring site. *Deep-Sea Res. Part I Oceanogr. Res. Pap.* **54**: 608–636. doi:[10.1016/j.dsr.2006.12.011](https://doi.org/10.1016/j.dsr.2006.12.011)

- Kostaschuk, R., J. Best, P. Villard, J. Peakall, and M. Franklin. 2005. Measuring flow velocity and sediment transport with an acoustic Doppler current profiler. *Geomorphology* **68**: 25–37. doi:[10.1016/j.geomorph.2004.07.012](https://doi.org/10.1016/j.geomorph.2004.07.012)
- Kubaneck, J., T. W. Snell, and C. Pirkle. 2007. Chemical defense of the red tide dinoflagellate *Karenia brevis* against rotifer grazing. *Limnol. Oceanogr.* **52**: 1026–1035. doi:[10.4319/lo.2007.52.3.1026](https://doi.org/10.4319/lo.2007.52.3.1026)
- La, H. S., H. K. Ha, C. Y. Kang, A. K. Wählin, and H. C. Shin. 2015. Acoustic backscatter observations with implications for seasonal and vertical migrations of zooplankton and nekton in the Amundsen shelf (Antarctica). *Estuar. Coast. Shelf Sci.* **152**: 124–133. doi:[10.1016/j.ecss.2014.11.020](https://doi.org/10.1016/j.ecss.2014.11.020)
- Lampert, W. 1989. The adaptive significance of diel vertical migration of zooplankton. *Funct. Ecol.* **3**: 21–27. doi:[10.2307/2389671](https://doi.org/10.2307/2389671)
- Lavery, A. C., P. H. Wiebe, T. K. Stanton, G. L. Lawson, M. C. Benfield, and N. Copley. 2007. Determining dominant scatterers of sound in mixed zooplankton populations. *J. Acoust. Soc. Am.* **122**: 3304–3326. doi:[10.1121/1.2793613](https://doi.org/10.1121/1.2793613)
- Leonardsson, K. 1991. Predicting risk-taking behaviour from life-history theory using static optimization technique. *Oikos* **60**: 149–154. doi:[10.2307/3544860](https://doi.org/10.2307/3544860)
- Lester, K. M., and others. 2008. Zooplankton and *Karenia brevis* in the Gulf of Mexico. *Cont. Shelf Res.* **28**: 99–111. doi:[10.1016/j.csr.2007.04.009](https://doi.org/10.1016/j.csr.2007.04.009)
- Loose, C. J., and P. Dawidowicz. 1994. Trade-offs in diel vertical migration by zooplankton: The costs of predator avoidance. *Ecology* **75**: 2255–2263. doi:[10.2307/1940881](https://doi.org/10.2307/1940881)
- Lu, Y., and R. G. Lueck. 1999. Using a broadband ADCP in a Tidal Channel. Part II: Turbulence. *J. Atmos. Ocean. Technol.* **16**: 1568–1579. doi:[10.1175/1520-0426\(1999\)016<1568:UABAIA>2.0.CO;2](https://doi.org/10.1175/1520-0426(1999)016<1568:UABAIA>2.0.CO;2)
- Lyczkowski-Shultz, J., and J. P. Steen. 1991. Diel vertical distribution of red drum *Sciaenops ocellatus* larvae in the north-central Gulf of Mexico. *Fish. Bull.* **89**: 631–641.
- Macquart-Moulin, C. 1999. Diel vertical migration and endogenous swimming rhythm in *Asterope mariae* (Baird) and *Philomedes interpuncta* (Baird) (Crustacea Ostracoda Cypridinidae). *J. Plankton Res.* **21**: 1891–1910. doi:[10.1093/plankt/21.10.1891](https://doi.org/10.1093/plankt/21.10.1891)
- Mahoney, K. L. 2003. Backscattering of light by *Karenia brevis* and implications for optical detection and monitoring. Univ. of Southern Mississippi.
- Mutlu, E. 1996. Target strength of the common jellyfish (*Aurelia aurita*): A preliminary experimental study with a dual-beam acoustic system. *ICES J. Mar. Sci.* **53**: 309–311. doi:[10.1006/jmsc.1996.0040](https://doi.org/10.1006/jmsc.1996.0040)
- Neilson, J. D., and R. I. Perry. 1990. Diel vertical migrations of marine fishes: An obligate or facultative process? *Adv. Mar. Biol.* **26**: 115–168. doi:[10.1016/S0065-2881\(08\)60200-X](https://doi.org/10.1016/S0065-2881(08)60200-X)
- Ochoa, J., H. Maske, J. Sheinbaum, and J. Candela. 2013. Diel and lunar cycles of vertical migration extending to below 1000 m in the ocean and the vertical connectivity of depth-tiered populations. *Limnol. Oceanogr.* **58**: 1207–1214. doi:[10.4319/lo.2013.58.4.1207](https://doi.org/10.4319/lo.2013.58.4.1207)
- Ott, M. W. 2005. The accuracy of acoustic vertical velocity measurements: Instrument biases and the effect of zooplankton migration. *Cont. Shelf Res.* **25**: 243–257. doi:[10.1016/J.CSR.2004.09.007](https://doi.org/10.1016/J.CSR.2004.09.007)
- Pagès, F., and J.-M. Gili. 1991. Vertical distribution of epipelagic siphonophores at the confluence between Benguela waters and the Angola Current over 48 hours, p. 355–362. *In* R. B. Williams, P. F. S. Cornelius, R. G. Hughes, and E. A. Robson [eds.], *Developments in hydrobiology*. Springer. doi:[10.1007/978-94-011-3240-4_51](https://doi.org/10.1007/978-94-011-3240-4_51)
- Paris, C. B., and R. K. Cowen. 2004. Direct evidence of a biophysical retention mechanism for coral reef fish larvae. *Limnol. Oceanogr.* **49**: 1964–1979. doi:[10.4319/lo.2004.49.6.1964](https://doi.org/10.4319/lo.2004.49.6.1964)
- Pearre, S. 2003. Eat and run? The hunger/satiation hypothesis in vertical migration: History, evidence and consequences. *Biol. Rev.* **78**: 1–79. doi:[10.1017/S146479310200595X](https://doi.org/10.1017/S146479310200595X)
- Perkins, H. T., F. de Strobel, and L. Gualdesi. 2000. The Barny Sentinel trawl-resistant ADCP bottom mount: Design, testing, and application. *IEEE J. Ocean. Eng.* **25**: 430–436. doi:[10.1109/48.895350](https://doi.org/10.1109/48.895350)
- Pinot, J. M., and J. Jansá. 2001. Time variability of acoustic backscatter from zooplankton in the Ibiza Channel (western Mediterranean). *Deep-Sea Res. Part I Oceanogr. Res. Pap.* **48**: 1651–1670. doi:[10.1016/S0967-0637\(00\)00095-9](https://doi.org/10.1016/S0967-0637(00)00095-9)
- Plueddemann, A. J., and R. Pinkel. 1989. Characterization of the patterns of diel migration using a Doppler sonar. *Deep-Sea Res.* **36**: 509–530. doi:[10.1016/0198-0149\(89\)90003-4](https://doi.org/10.1016/0198-0149(89)90003-4)
- Prihartato, P. K., X. Irigoien, M. G. Genton, and S. Kaartvedt. 2016. Global effects of moon phase on nocturnal acoustic scattering layers. *Mar. Ecol. Prog. Ser.* **544**: 65–75. doi:[10.3354/meps11612](https://doi.org/10.3354/meps11612)
- Qi, L., C. Hu, B. B. Barnes, and Z. Lee. 2017. VIIRS captures phytoplankton vertical migration in the NE Gulf of Mexico. *Harmful Algae* **66**: 40–46. doi:[10.1016/j.hal.2017.04.012](https://doi.org/10.1016/j.hal.2017.04.012)
- Rasband, W. S. 2012. ImageJ: Image processing and analysis in Java. *Astrophys. Source Code Libr.* **1**: 6013.
- Remsen, A. W., T. L. Hopkins, and S. Samson. 2004. What you see is not what you catch: A comparison of concurrently collected net, optical plankton counter, and shadowed image particle profiling evaluation recorder data from the Northeast Gulf of Mexico. *Deep-Sea Res. Part I Oceanogr. Res. Pap.* **51**: 129–151. doi:[10.1016/j.dsr.2003.09.008](https://doi.org/10.1016/j.dsr.2003.09.008)
- Rimmer, D. W., and B. F. Phillips. 1979. Diurnal migration and vertical distribution of phyllosoma larvae of the western rock lobster *Panulirus cygnus*. *Mar. Biol.* **54**: 109–124. doi:[10.1007/BF00386590](https://doi.org/10.1007/BF00386590)
- Schiller, R. V., V. H. Kourafalou, P. Hogan, and N. D. Walker. 2011. The dynamics of the Mississippi River plume: Impact of topography, wind and offshore forcing on the fate of plume waters. *J. Geophys. Res. Oceans* **116**: C06029. doi:[10.1029/2010JC006883](https://doi.org/10.1029/2010JC006883)

- Sindlinger, L. R., D. C. Biggs, and S. F. Dimarco. 2005. Temporal and spatial variability of ADCP backscatter on a continental slope. *Cont. Shelf Res.* **25**: 259–275. doi:[10.1016/j.csr.2004.10.002](https://doi.org/10.1016/j.csr.2004.10.002)
- Soto, I. M., J. P. Cannizzaro, F. E. Muller-Karger, C. Hu, J. Wolny, and D. Goldgof. 2015. Evaluation and optimization of remote sensing techniques for detection of *Karenia brevis* blooms on the West Florida shelf. *Remote Sens. Environ.* **170**: 239–254. doi:[10.1016/j.rse.2015.09.026](https://doi.org/10.1016/j.rse.2015.09.026)
- Soto, I. M., and others. 2018. Advection of *Karenia brevis* blooms from the Florida panhandle towards Mississippi coastal waters. *Harmful Algae* **72**: 46–64. doi:[10.1016/j.hal.2017.12.008](https://doi.org/10.1016/j.hal.2017.12.008)
- Stanton, T. K., and D. Chu. 2000. Review and recommendations for the modelling of acoustic scattering by fluid-like elongated zooplankton: Euphausiids and copepods. *ICES J. Mar. Sci. J. Cons.* **57**: 793–807. doi:[10.1006/jmsc.1999.0517](https://doi.org/10.1006/jmsc.1999.0517)
- Stich, H.-B., and W. Lampert. 1981. Predator evasion as an explanation of diurnal vertical migration by zooplankton. *Nature* **293**: 396–398. doi:[10.1038/293396a0](https://doi.org/10.1038/293396a0)
- Tarling, G. A., T. Jarvis, S. M. Emsley, and J. B. L. Matthews. 2002. Midnight sinking behaviour in *Calanus finmarchicus*: A response to satiation or krill predation? *Mar. Ecol. Prog. Ser.* **240**: 183–194. doi:[10.3354/meps240183](https://doi.org/10.3354/meps240183)
- Teledyne, R. D. I. 2011. Acoustic Doppler current profiler principles of operation: A practical primer. P/N 951-6069-00; [accessed 2019 February 1]. Available from <http://www.teledynemarine.com/Documents/Forms/AllItems.aspx>
- Torrence, C., and G. P. Compo. 1998. A practical guide to wavelet analysis. *Bull. Am. Meteorol. Soc.* **79**: 61–78. doi:[10.1175/1520-0477\(1998\)079<0061:APGTWA>2.0.CO;2](https://doi.org/10.1175/1520-0477(1998)079<0061:APGTWA>2.0.CO;2)
- Trevorrow, M. V., D. L. Mackas, and M. C. Benfield. 2005. Comparison of multifrequency acoustic and in situ measurements of zooplankton abundances in Knight Inlet, British Columbia. *J. Acoust. Soc. Am.* **117**: 3574–3588. doi:[10.1121/1.1920087](https://doi.org/10.1121/1.1920087)
- Turner, J. T., and P. A. Tester. 1989. Zooplankton feeding ecology: Copepod grazing during an expatriate red tide, p. 359–374. *In* E. M. Coper, V. M. Bricelj, and E. J. Carpenter [eds.], *Novel phytoplankton blooms*. Springer. doi:[10.1007/978-3-642-75280-3_21](https://doi.org/10.1007/978-3-642-75280-3_21)
- Valle-Levinson, A., L. Castro, M. Cáceres, and O. Pizarro. 2014. Twilight vertical migrations of zooplankton in a Chilean fjord. *Prog. Oceanogr.* **129**: 114–124. doi:[10.1016/j.pocean.2014.03.008](https://doi.org/10.1016/j.pocean.2014.03.008)
- van Haren, H. 2007. Monthly periodicity in acoustic reflections and vertical motions in the deep ocean. *Geophys. Res. Lett.* **34**: L12603. doi:[10.1029/2007GL029947](https://doi.org/10.1029/2007GL029947)
- van Haren, H., and T. J. Compton. 2013. Diel vertical migration in deep sea plankton is finely tuned to latitudinal and seasonal day length. *PLoS One* **8**: e64435. doi:[10.1371/journal.pone.0064435](https://doi.org/10.1371/journal.pone.0064435)
- Warren, J. D., T. K. Stanton, M. C. Benfield, P. H. Wiebe, D. Chu, and M. Sutor. 2001. In situ measurements of acoustic target strengths of gas-bearing siphonophores. *ICES J. Mar. Sci.* **58**: 740–749. doi:[10.1006/jmsc.2001.1047](https://doi.org/10.1006/jmsc.2001.1047)
- Wiebe, P. H., L. P. Madin, L. R. Hauray, G. R. Harbison, and L. M. Philbin. 1979. Diel vertical migration by *Salpa aspera* and its potential for large-scale particulate organic matter transport to the deep-sea. *Mar. Biol.* **53**: 249–255. doi:[10.1007/BF00952433](https://doi.org/10.1007/BF00952433)
- Wiebe, P. H., and C. H. Greene. 1994. The use of high frequency acoustics in the study of zooplankton spatial and temporal patterns. *Proc. NIPR Symp. Polar Biol.* **7**: 133–157. doi:[10.1037/0022-006X.62.6.1204](https://doi.org/10.1037/0022-006X.62.6.1204)
- Winder, M., J. Carstensen, A. W. E. Galloway, H. H. Jakobsen, and J. E. Cloern. 2017. The land–sea interface: A source of high-quality phytoplankton to support secondary production. *Limnol. Oceanogr.* **62**: S258–S271. doi:[10.1002/lno.10650](https://doi.org/10.1002/lno.10650)
- Wong, D. W. S., and J. Lee. 2005. *Statistical analysis of geographic information with ArcView GIS and ArcGIS*. John Wiley.

Acknowledgments

We appreciate the suggestions from the two anonymous reviewers that improved the quality of the manuscript. Thank you to everyone involved in CONCORDE, and the crews of the research vessels *Point Sur* and *Pelican*. This research was made possible by a grant from The Gulf of Mexico Research Initiative. Data are publicly available through the Gulf of Mexico Research Initiative Information and Data Cooperative at <https://data.gulfresearchinitiative.org>, doi:[10.7266/N79C6VGW](https://doi.org/10.7266/N79C6VGW) (ADCPs); doi:[10.7266/N77D2SRV](https://doi.org/10.7266/N77D2SRV) (wave and tide gauges); doi:[10.7266/n7-yan1-f697](https://doi.org/10.7266/n7-yan1-f697) (ISIS); doi:[10.7266/N7XP730K](https://doi.org/10.7266/N7XP730K) (net samples); doi:[10.7266/N73T9FNX](https://doi.org/10.7266/N73T9FNX) (satellite data); and doi:[10.7266/N7XD103N](https://doi.org/10.7266/N7XD103N) (glider). S. M. Parra is grateful for funding provided from the U.S. Naval Research Laboratory through an American Society for Engineering Education postdoctoral fellowship. We thank the NASA Goddard Space Flight Center, Ocean Ecology Laboratory, Ocean Biology Processing Group for the moderate-resolution Imaging Spectroradiometer Aqua ocean color data and 2014 Reprocessing (NASA OB.DAAC, Greenbelt, Maryland; doi:[10.5067/AQUA/MODIS/MODIS_OC.2014.0](https://doi.org/10.5067/AQUA/MODIS/MODIS_OC.2014.0)).

Conflict of Interest

None declared

Submitted 11 July 2018

Revised 04 March 2019

Accepted 15 March 2019

Associate editor: Kelly Benoit-Bird